Addendum to the MINERνA Proposal: Updates to the Physics Case for MINERνA

April 2, 2004

Abstract

The MINERνA collaboration has proposed to construct a new detector to perform a high-statistics, high-resolution ν and $\overline{\nu}$–nucleon/nucleus scattering experiment in the NuMI beamline. In this document, we expand upon the physics justification for the experiment already described in the proposal.

The MINERνA Collaboration

D. Drakoulakos, P. Stamoulis, G. Tzanakos, M. Zois
University of Athens; Athens, Greece

D. Casper
University of California, Irvine; Irvine, California, USA

E. Paschos
University of Dortmund, Dortmund, Germany

D. Boehnlein, D. Harris, M. Kostin, J.G. Morfín*, P. Shanahan
Fermi National Accelerator Laboratory; Batavia, Illinois, USA

M.E. Christy, W. Hinton, C.E. Keppel[1]
Hampton University; Hampton, Virginia, USA

R. Burnstein, A. Chakravorty[2], O. Kamaev, N. Solomey
Illinois Institute of Technology; Chicago, Illinois, USA

S. Kulagin
Institute for Nuclear Research, Moscow, Russia

W.K. Brooks, A. Bruell, R. Ent, D. Gaskell, W. Melnitchouk, S.A. Wood
Thomas Jefferson National Accelerator Facility; Newport News, Virginia, USA

I. Niculescu, G. Niculescu
James Madison University, Harrisonburg, Virginia, USA

G. Blazey, M.A.C. Cummings, V. Rykalin
Northern Illinois University; DeKalb, Illinois, USA

S. Boyd, D. Naples, V. Paolone
University of Pittsburgh; Pittsburgh, Pennsylvania, USA

A. Bodek, H. Budd, J. Chvojka, P. deBarbaro, S. Manly, K. McFarland*, I. Park, W. Sakumoto, R. Teng
University of Rochester; Rochester, New York, USA

R. Gilman, C. Glashausser, X. Jiang, G. Kumbartzki, K. McCormick, R. Ransome
Rutgers, The State University of New Jersey; Piscataway, New Jersey, USA

H. Gallagher, T. Kafka, W.A. Mann, W. Oliver
Tufts University; Boston, Massachusetts, USA

[1] Also at Thomas Jefferson National Accelerator Facility
[2] Also at Saint Xavier College, Chicago, Illinois, USA
* Co-spokespersons

Contents

List of Tables

List of Figures

1 Introduction

As detailed in the MINERνA proposal, the imminent completion of the NUMI beamline offers the particle and nuclear physics communities a new opportunity to study neutrino interactions in an environment unprecedented in granularity of detectors and event rate. The construction of MINERνA, with its fully active core target, would allow a wide variety of measurements in neutrino interaction physics, which both support future and current neutrino oscillation efforts, and are interesting for their own sake.

Since the proposal was submitted to the FNAL PAC at the December 2003 meeting, the MINERνA collaboration has continued to make progress in understanding the ultimate capabilities of the experiment. This addendum serves to document these continuing studies for the benefit of the PAC as we seek approval of the experiment.

This document is broken down by physics topic, and each section contains a brief summary of the physics goals, the status of our understanding at the time of the proposal, and then documents improved understanding, since the proposal, in more detail. The topics considered in this addendum are:

- Quasi-Elastic Cross-Sections and Form Factors
- Coherent Pion Production
- Physics Opportunities in the Resonance Production Region
- Nuclear Effects in Neutrino Scattering
- The Impact of MINERνA on Oscillation Experiments

This document is intended to be read as a supplement to the updated MINERνA proposal [1]. This document, along with other documentation of the status of the MINERνA experiment, is available from the MINERνA collaboration web page, `http://www.pas.rochester.edu/minerva/`

2 Quasi-Elastic Scattering

At the lowest neutrino energies relevant for future long baseline efforts, it is the quasi-elastic scattering that dominates the charged current interaction rate. As outlined in the MINERνA proposal[1], there are some interesting physics issues to be addressed in quasi-elastic neutrino scattering. The first of these is understanding the impact of nuclear effects on the quasi-elastic kinematics at low Q^2 which dominates the signal rate for oscillation experiments. The second is understanding the axial form-factor of the proton at high Q^2 which will contribute to the blossoming body of new measurements on high Q^2 nucleon form-factors where some surprises have already been seen in charged-lepton scattering (see MINERνA proposal). Since the proposal, we have made significant progress in simulating our expected analysis of quasi-elastics, focusing on the important issues of maintaining high efficiency at low Q^2 and low backgrounds at high Q^2.

In $\nu n \rightarrow \mu^- p$, the outgoing proton carries a kinetic energy that is approximately $Q^2/2M_N$. So for low Q^2, the challenge is identifying events with a very soft recoil proton; for high Q^2, this proton is high energy and may interact in the detector, making particle identification more challenging. The main strategies of the current analysis are:

- At low Q^2, accept quasi-elastic candidates with a single (muon) track, and discriminate from background by requiring low activity in the remainder of the detector
- At high Q^2, reconstruct both the proton and the muon, and require kinematic consistency with $x = 1$ and $p_T = 0$

Simple cuts deriving from these ideas allow for reasonable efficiency with good purity, even at high Q^2.

2.1 Details of Quasi-elastic reconstruction

The analysis uses the NEUGEN generation and the hit level MINERνA simulation and tracking package in order to simulate signal selection and background processes.

The initial event identification proceeds by requiring one or two tracks in the active target. One of these tracks must be long range (400 g/cm^2) and is the

[1] see the discussion in Chapter 6 of the MINERνA proposal[1]

putative muon. If a second track forms a vertex with this track, it is assumed to be the proton. No other tracks are allowed to be connected with this event vertex. The muon track momentum is reconstructed with a fractional uncertainty of between 10–20%.

In the low Q^2 case, the proton track (if found) would be effectively required to lose energy by range since only a limited amount of detector activity not associated with the primary tracks is allowed by the event selection. We attempt to recover some of the lost efficiency at higher Q^2 due to this cut by allowing hits on tracks near the proton track to be associated with the proton track itself. Figure 1 shows the fraction of hits not associated with the lepton or proton in the quasi-elastic events and in expected background processes. For higher Q^2 events a similar requirement could in principle be applied, but it is not particularly effective nor efficient.

The energy of the proton for the high Q^2 case (where the proton almost always interacts) is reconstructed calorimetrically with an expected fractional energy resolution that is well parameterized by $35\%/\sqrt{E_{proton}}$.

Although muons are identified by requiring a single track with a long range in the detector, no attempt is made in the analysis to improve particle identification by requiring dE/dx consistent with the muon or proton tracks. This requirement is expected to be particularly effective for protons of $\mathcal{O}(1)$ GeV momentum[2], and such a requirement can be optimized to improve the analysis in the future. In addition, it may be possible to improve the efficiency by allowing a lower range muon with a dE/dx requirement without sacrificing purity.

If a quasi-elastic interaction is assumed, one can reconstruct the event kinematics from only the momentum and direction of the final state μ. Neglecting the binding energy of the final state proton,

$$E_\nu^{QE} = \frac{M_N E_\mu - \frac{m_\mu^2}{2}}{M_N - E_\mu + p_\mu \cos\theta_\mu}.$$

If a proton track is required and its angle and energy are measured, one can additionally require consistency with the quasi-elastic hypothesis. Two constraints are possible, one on the x of the reconstructed interaction and one on the p_T of the observed final state.

If the interaction is truly quasi-elastic, then $x = 1$, and therefore $Q^2 = 2M_N\nu$ where $\nu = E_{had} - M_{nucleon}$, and E_{had} is the energy of the hadronic final state. In this

[2] see Section 15.5.5 of the MINERνA proposal[1]

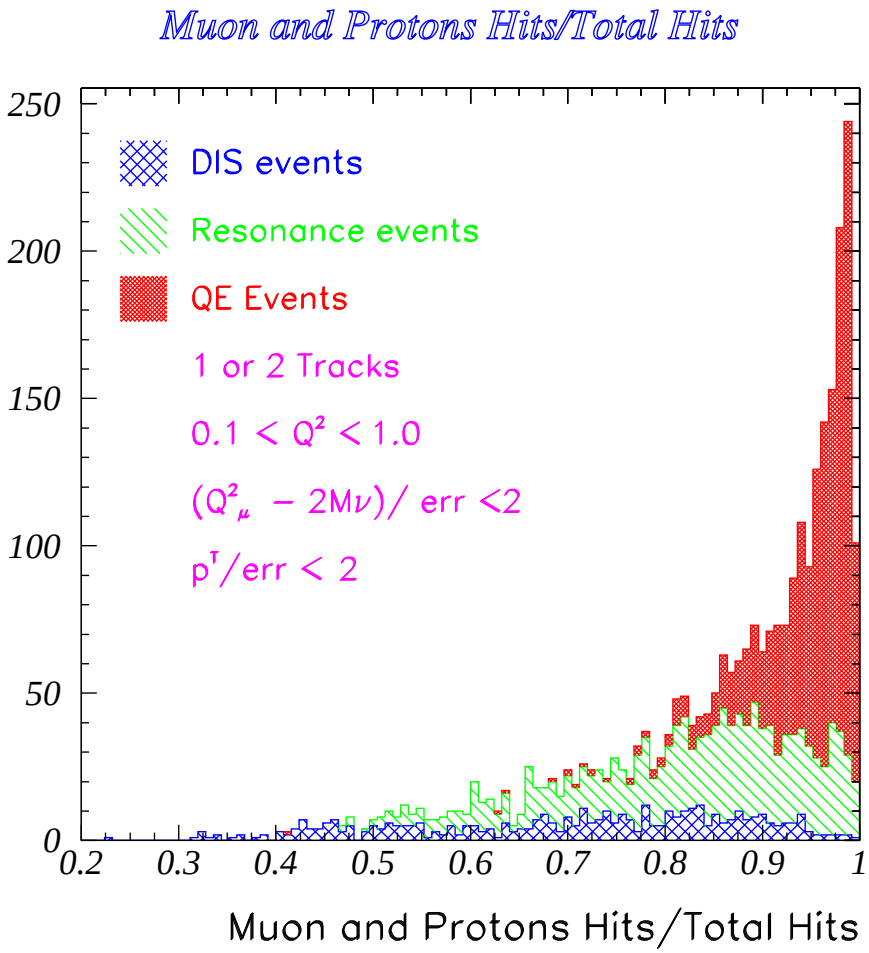

Figure 1: The fraction of hits associated with the muon and the proton tracks in quasi-elastic candidates. The events for the plot may have have one or two vertex tracks, pass additional kinematic requirement and are required to have $0.1\ GeV^2 < Q^2 < 1\ GeV^2$.

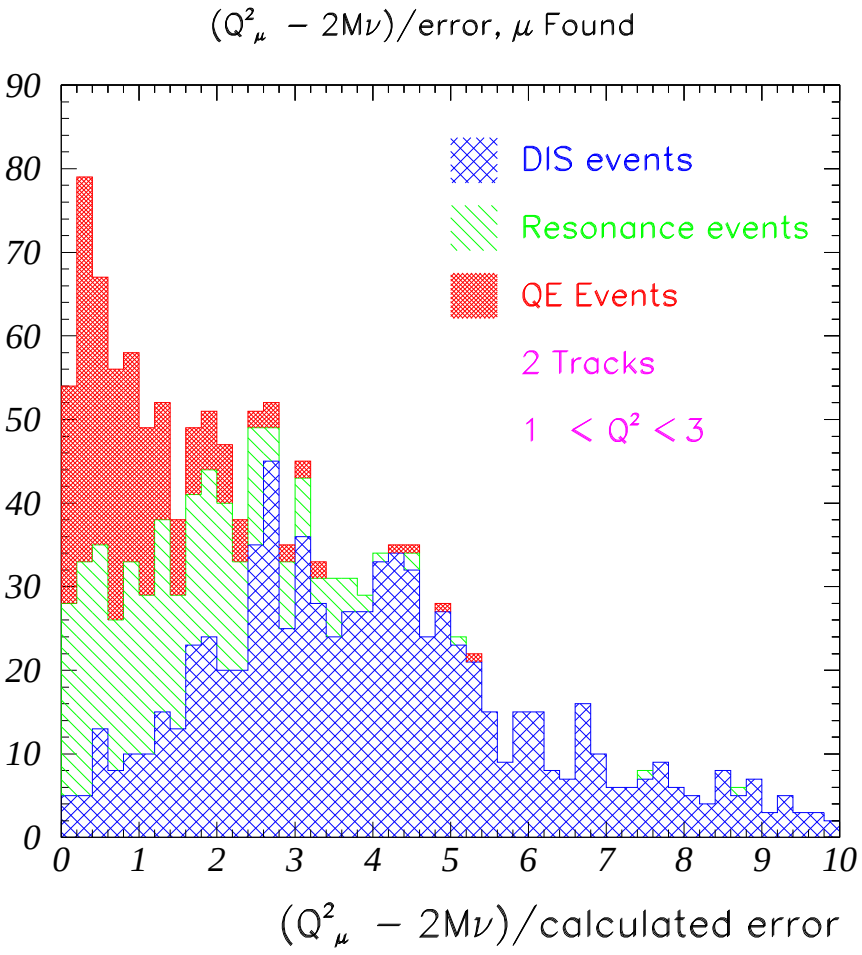

Figure 2: The significance of the difference between Q^2 from the quasi-elastic hypothesis and Q^2 from the final state energy

analysis, we test this by comparing Q^2 reconstructed from the lepton kinematics under the quasi-elastic hypothesis to $2M_N\nu$ and forming $(Q^2_\mu - 2M_N\nu)/error$ where the dominant part of the calculated error for this term comes from the smearing of hadronic final state energy. Figure 2 shows this Q^2 difference significance for two track quasi-elastic candidates with observed $1\ GeV^2 < Q^2 < 3\ GeV^2$, for quasi-elastic, resonance and DIS events. Note that this cut can be applied without identifying a proton track if the visible energy, less the muon energy, is assumed to be ν.

The Q^2 significance (x) cut does not use information on the proton direction, and so we impose a second kinematic cut on the p^T of the final state relative to the incoming neutrino direction. This selection requires that a proton track is identified and we cut on the significance of the difference from $p_T = 0$. We impose a cut of $p^T/error$ <2 except for $Q^2 > 3\ GeV^2$, for which the cut is 3. Note also that if we impose a p^T cut first, the Q^2 difference cut still improves the result, i.e. both cuts are needed.

In summary, the selection requirements for quasi-elastic candidates are:

- One or two tracks for $Q^2 < 1\ GeV^2$ and two tracks for $Q^2 > 1\ GeV^2$.
- One track must have 400 g/cm^2 range (muon).
- $(Q^2_\mu - 2M\nu)/(error) < 2$.
- $p_T/(error) < 2$ for $Q^2 < 3\ GeV^2$ and $p_T/(error) < 3$ for $Q^2 > 3\ GeV^2$.
- Hit fraction associated with muon and proton > 0.9, for $Q^2 < 0.5\ GeV^2$, or $>$ 0.85, for $0.5\ GeV^2 < Q^2 < 1.0\ GeV^2$.

2.2 Results

Table 1 shows the efficiency and purity of the quasi-elastic sample for different Q^2 bins after each cut. Using the calculated efficiency and purity, we have updated the uncertainties on F_A derived in the MINERνA proposal[1] which did not include efficiency or background effects.

Figure 3 shows the extracted values and errors on F_A in bins of Q^2 from a sample of simulated quasi-elastic interactions in the MINERνA active carbon target, for a four-year exposure in the NuMI beam. Figure 4 shows these results as a ratio of F_A/F_A(Dipole), demonstrating MINERνA's ability to distinguish between different models of F_A. Note that resolution effects are still not included in

	μ		$(Q^2_\mu - 2M\nu)$/err		p_T /err		Hits	
Q^2 bin	Effic	Purity	Effic	Purity	Effic	Purity	Effic	Purity
0.1-0.5	0.926	0.246	0.918	0.442	0.866	0.559	0.775	0.842
0.5 - 1	0.775	0.199	0.765	0.410	0.624	0.486	0.528	0.685
1 - 2	0.600	0.199	0.541	0.416	0.397	0.555	0.338	0.598
2 - 3	0.456	0.146	0.400	0.375	0.344	0.554	0.278	0.676
3 - 10	0.689	0.123	0.600	0.310	0.467	0.420	0.311	0.700

Table 1: Efficiency and purity in Q^2 bins for quasi-elastic candidates

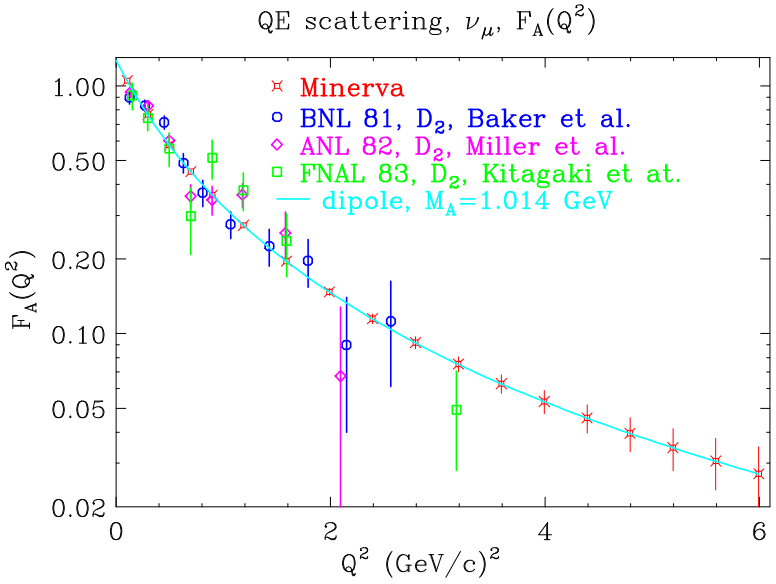

Figure 3: Estimation of F_A from a sample of Monte Carlo neutrino quasi-elastic events recorded in the MINERνA active carbon target. Here, a pure dipole form for F_A is assumed, with $M_A = 1.014$ GeV$/c^2$. The simulated sample and error bars correspond to four years of NuMI running. Also shown is F_A extracted from deuterium bubble chamber experiments using the $d\sigma/dq^2$ from the papers of FNAL 1983 [2] BNL 1981 [3], and ANL 1982 [4]

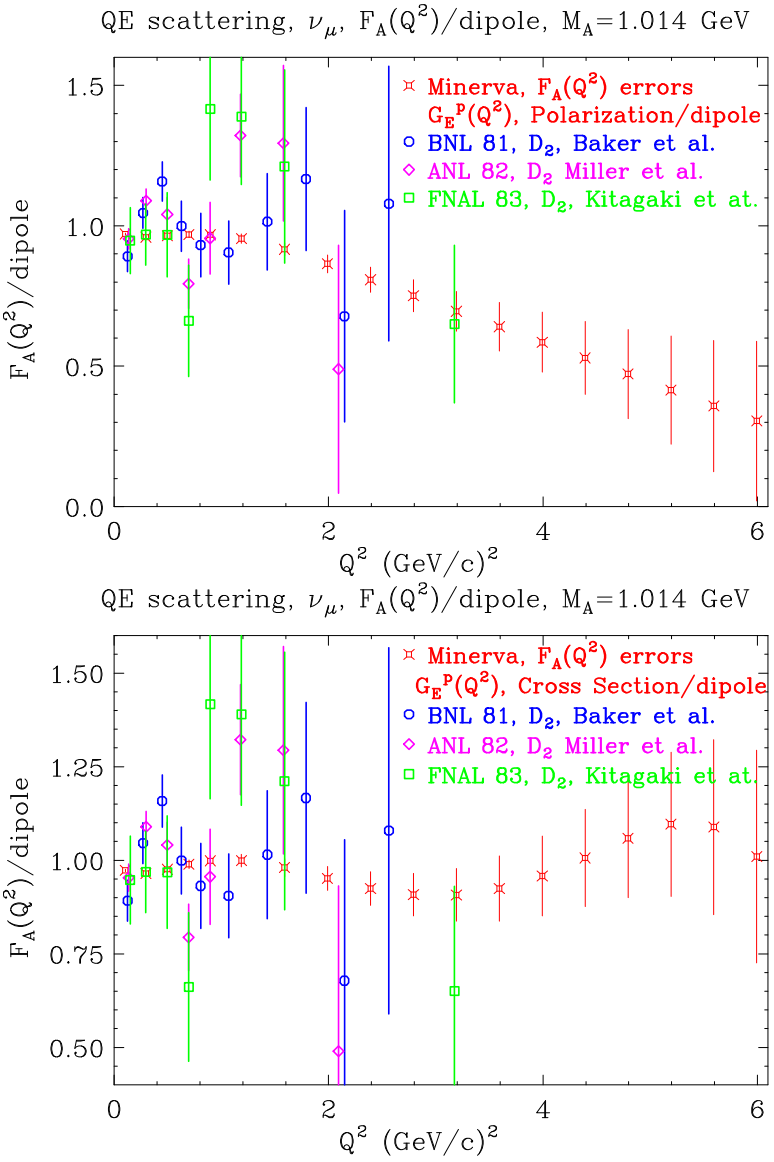

Figure 4: Extracted ratio F_A/F_A(Dipole) from MINERνA active target (4 NuMI-years) under two scenarios for the true F_A. **(Top)** F_A/F_A(Dipole) is G_E^p/G_E^p(dipole) from polarization transfer measurements. **(Bottom)** F_A/F_A(Dipole) is G_E^p/G_E^p(dipole) from Rosenbluth separation technique. Also shown is F_A extracted from deuterium bubble chamber experiments using the $d\sigma/dq^2$ from the papers of FNAL 1983 [2] BNL 1981 [3], and ANL 1982 [4]

this extraction of F_A; however, the typical Q^2 resolution for quasi-elastic events at high Q^2 is $\lesssim 0.2$ GeV^2 which is smaller than the bin size.

3 Coherent Neutrino-Nucleus Scattering

With its high statistics, fine segmentation, excellent tracking, good particle ID, and range of nuclear targets, the MINERνA experiment will be able to obtain data samples of coherent interactions several orders of magnitude larger than those published from previous experiments. The study of neutrino coherent scattering is an excellent tool for exploring the 'hadronic' nature of the weak current, particularly the axial component.

The capabilities of MINERνA for coherent scattering are compelling for a number of reasons:

1. Coherent π production is largely a neutrino-specific process, as the coupling is dominated by axial current. In the Rein-Seghal model [9], for instance, the coupling is entirely axial. Therefore there is no electron-scattering analogue to constrain models for this process.

2. Existing measurements in the energy range of the NuMI beam are quite poor. There is only one experiment (SKAT) with data on charged current coherent production below E_ν of 10 GeV, and it only had 59 events.

3. The charged current is an extremely clean measurement in MINERνA because distinct muon and pion tracks will be clearly visible and will allow precise measurement of the interaction point and kinematic quantities.

4. With nuclear targets spanning A=12 to A=207, MINERνA will be the first experiment to measure the A-dependence of the coherent cross section.

5. An improved knowledge of coherent cross sections will be crucial for future oscillation experiments, as the neutral current reaction producing a single π^0 is one of the main backgrounds for subdominant $\nu_\mu \rightarrow \nu_e$ mixing searches.

6. The π^0 reconstruction capabilities of MINERνA make it possible to statistically separate coherent from non-coherent π^0 production to directly determine this background and to check the expected relationship to the charged-current process.

MINERνA selects coherent events in both the charged and neutral current by relying on the distinct kinematics of the events. Because the coherence condition requires that the nucleus remain intact, the process is tagged by low-energy transfer ($|t|$) to the nuclear system which is reconstructed by

$$-|t| = -(q - p_\pi)^2 = (\Sigma_i(E_i - p_i^{||}))^2 - (\Sigma_i(p_i^{\perp}))^2. \quad (1)$$

Cut	Signal Sample	Background Sample
	5000	10000
2 Charged Tracks	3856	3693
Track Identification	3124	3360
π^o/neutron Energy	3124	1744
Track Separation	2420	500
x<0.2	2223	100
t<0.2	2223	19
$p_\pi < 600$ MeV	1721	12

Table 2: Analysis cuts to isolate a sample of coherent interactions. The cuts are described in the text.

Candidate events are generally selected as coherent by requiring a low final state multiplicity and by requiring kinematics consistent with low $|t|$.

The MINERνA event selection is described in detail in the proposal[3]. The efficiency and purity of the selection in the charged current case is summarized in Table 3, and the expected uncertainties in the final cross-section as a function of energy is shown in Figure 5.

3.1 A-Dependence of the Cross Section

As noted above, there are no existing measurements of the coherent cross-sections on light nuclei (e.g., H, C, O). These measurements are important for planned ν_e appearance experiments. Current predictions must rely on extrapolation in A in addition to extrapolation to lower energies.

Figure 6 shows the predicted A-dependence of the charged current coherent cross section from Rein-Seghal and Paschos-Kartavtsev [9, 10] models, and the expected measurement errors from MINERνA. As this analysis indicates, the high statistics and large dynamic range in A of the MINERνA experiment will make possible detailed examinations of the coherently produced meson-nucleus interaction. Although K2K and MiniBooNE are expected to significantly improve the knowledge of coherent π production on CH_n at very low energies, only MINERνA will be able to reach this level of precision and to perform this systematic examination of the A dependence of the cross-section.

[3]Chapter 8 of the MINERνA proposal [1]

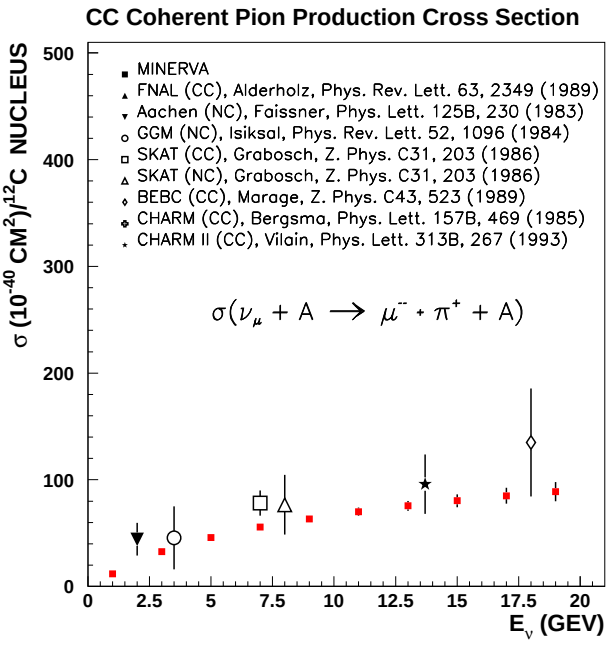

Figure 5: Coherent cross-sections as measured by MINERνA compared with existing published results. MINERνA errors here are statistical only, and the assumed true value is that predicted by Rein-Seghal [9].

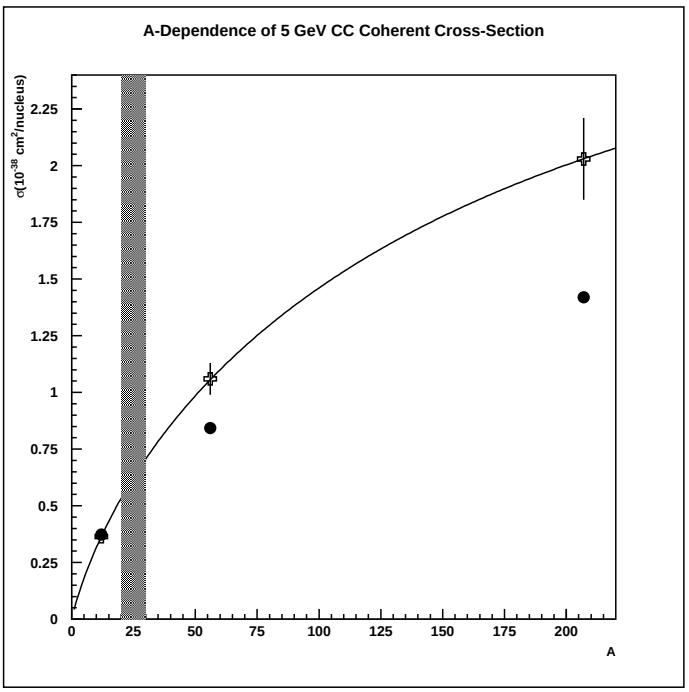

Figure 6: Coherent cross-sections for 5 GeV neutrinos as a function of atomic number. Solid curve is the prediction of Rein-Seghal, solid circles are the predictions of Paschos-Kartavtsev for carbon, iron and lead. Crosses indicate the expected measurement errors for minerva assuming the measured cross section is that of Rein-Seghal. The shaded band indicates the region explored in previous experiments, primarily from measurements on aluminum (A=27), neon (A=20), and freon (<A>=30), all performed at higher energies than are relevant for MINERνA or future oscillation experiments.

4 Measuring Nuclear Effects with the MINERνA Detector

As indicated in our proposal, to study nuclear effects in MINERνA, carbon, iron and lead targets will be installed upstream of the pure scintillator active detector. The currently preferred configuration involves a total of 6 planes, with each plane divided transversely into C, Fe and Pb wedges. As one proceeds from upstream to downstream, the C, Fe and Pb targets exchange (rotate) positions. As always, a scintillator module of four views (x,u,x,v) separates each of the planes. The total mass is over 1 ton of Fe and Pb and somewhat over 0.5 ton of C. Since the pure scintillator active detector essentially acts as an additional 3-ton carbon target (CH), the pure graphite (C) target is mainly to check for consistency. For the standard four-year run described in the proposal, MINERνA would collect 1 M events on Fe and Pb, 600 k events on C as well as 2.8 M events on the scintillator within the fiducial volume. In this section we give more experimental background than was given in the proposal[4], as well as describe more specifically the analysis technique that will be used to measure nuclear effects.

MINERνA's goals in measuring nuclear effects can be summarized as follows:

- measure final-state multiplicities, and hence absorption probabilities, as a function of A with initial ν;
- measure the visible hadron energy distribution as a function of target nucleus to determine the relative energy loss due to final state interactions (FSI);
- investigate if the correction factors for observed multiplicity and hadron energy are a function of the muon kinematics for a more directed application of nuclear effect corrections.
- measure $\sigma(x_{Bj})$ for each nuclear target to compare x_{Bj}-dependent nuclear effects measured with both ν and charged lepton beams.
- If sufficient $\overline{\nu}$ running is available, measure the nuclear effects on $F_2(x,Q^2)$ and $xF_3(x,Q^2)$ to determine whether sea and valence quarks are affected differently by the nuclear environment.

[4] see Chapter 12 of the MINERνA proposal [1]

4.1 Pion Absorption Effects in Neutrino Interactions

Interactions of few GeV neutrinos in nuclei easily produce resonances which decay to pions. Any attempt to reconstruct the incident neutrino energy based on the total observed energy must take into account the interactions of the pions in both the interaction nucleus and the detector. Current neutrino interaction Monte Carlos (such as INTRANUKE [11]) handle pion interactions crudely and have generally not yet incorporated the latest knowledge of pion interactions. We would like to summarize here the current knowledge of pion interactions and discuss plans for using MINERνA to better account for pion interactions for neutrino-nucleus interactions.

Our concern here is mainly with pions in the energy range of 100 to 500 MeV, where the interaction cross sections are the highest. In this range the pion-nucleon cross section is dominated by the very strong $\Delta(1232)$ resonance. The Δ is a fairly broad (about 100 MeV) resonance, and the pion-nucleon cross section reflects this, with a peak near 200 MeV pion energy which drops quickly above and below this. The pion nucleus cross section exhibits a similar behavior, with a less pronounced drop-off at higher energy. The charged pion nucleus cross section has four important components in the intermediate energy range: elastic scattering (nucleus left in ground state), inelastic scattering (nucleus left in excited state or nucleon knocked out), true absorption (no pion in the final state), and single charge exchange (neutral pion in the final state).

Neutrino detectors are mainly iron (absorber), oxygen (water) and carbon (scintillator). The total pi-carbon cross section is 600 mb, with elastic and inelastic cross sections about 200 mb each, and absorption about 160 mb. The total pi-iron cross section is about 1700 mb, with elastic and absorption about 600 mb each, and inelastic about 400 mb. Cross sections for positive and negative pions are nearly the same because nuclei contain about the same number of protons and neutrons. These very large cross sections mean that essentially all pions will undergo some nuclear reaction, many within the interaction nucleus, and in most circumstances nearly all will be absorbed rather than stopping or exiting the detector. The absorption probability within the interaction nucleus is order 30% while the absorption probabilities in the detector are about 1%/cm in scintillator and 4%/cm in iron. Figure 7 [5] shows absorption cross sections for various nuclei as a function of pion energy.

In elastic and most inelastic reactions the scattered pion will not, because of its light mass, lose much energy. However, absorbed pions will lose all of their kinetic and mass energy. Most of that energy will go into nucleons. We want to

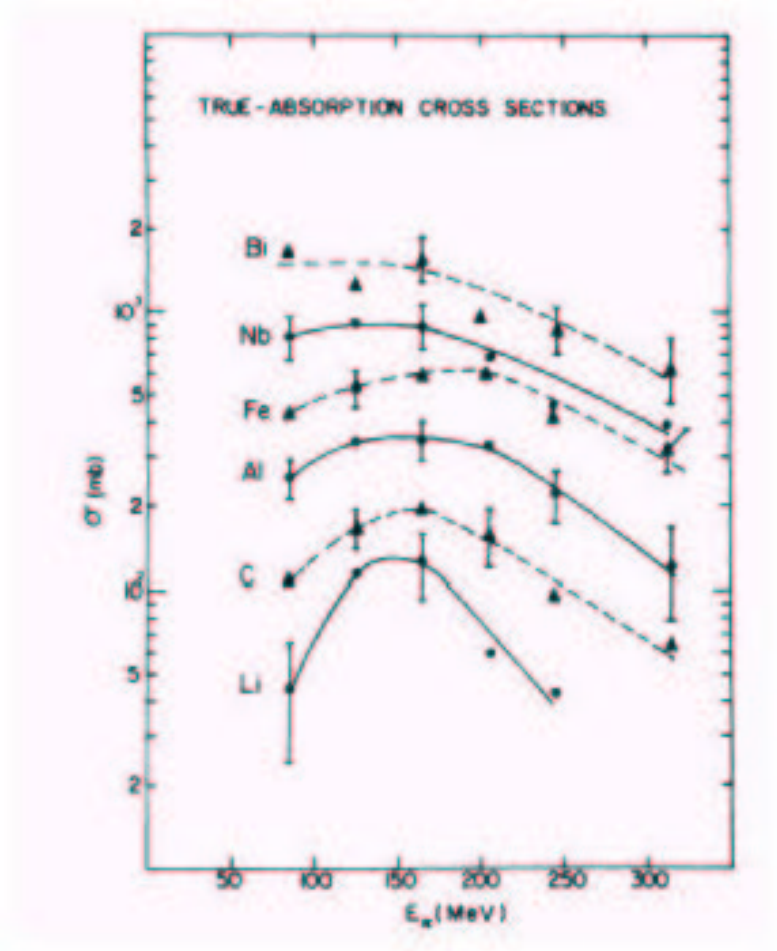

Figure 7: The absorption cross-sections for various nuclei as a function of pion energy.

discuss here what happens to that energy.

Pion absorption cannot occur on a single nucleon due to energy and momentum conservation. The simplest absorption mechanism is on two nucleons. Because absorption appears to proceed mainly through the $N-\Delta$ intermediate states, an isospin zero (np) pair is the primary candidate. Such an absorption for a positive pion would give two energetic protons whose kinetic energy nearly equaled the total pion energy. However, early studies of pion absorption found that was not the most probable mechanism.

In the 1990's two large solid angle detectors, the LAMPF BGO Ball and the PSI LADS detector, were built to study pion absorption. Both detectors had large solid angles (both more than 90% of the full solid angle) and low proton thresholds (about 20 MeV for each). The LADS detector also had reasonable neutron detection efficiency and energy measurement. The somewhat surprising result from both detectors was that pion absorption was dominated by three body absorption [6]. For positive pions, the absorption on a pnn triplet (leading to a ppn final state) was the most common. This was observed even in ^{4}He. The absorption in heavier nuclei also appears to proceed mainly through a three-body mechanism, although increased initial state interactions (pion re-scattering) and final state interactions (nucleon re-scattering) result in four to five nucleons being emitted. Typically the final state contains more neutrons than protons. The absorption process, which is still not well understood theoretically, largely fills the available phase space thus giving a wide range of nucleon energies with little angular dependence.

Because much of the energy is in neutrons, the observed energy is well below the total pion energy. Figure 8 and Figure 9 [7] show missing energy (total pion energy minus the total proton kinetic energy) for absorption of 250-500 MeV positive pions on ^{12}C and ^{58}Ni. As can be seen, even in carbon more than half the energy is lost to unobserved particles, a fraction which increases with pion energy and with A.

The situation is of course worse for negative pions. Charge symmetry would indicate that the primary absorption should be on a ppn triplet leading to a pnn final state. In this case, most of the pion energy would be in neutrons, and hence not directly observed. However, if the interaction vertex and one proton energy is known, and the angles of the outgoing neutrons are known, the total energy of the three nucleons can be estimated. Monte Carlo studies with realistic absorption models will be needed to determine the accuracies of such estimates.

Although neutral pions escaping the nucleus will decay, usually to two photons, the mean distance traveled before decay is a few nanometers, much greater than the size of the nucleus. Thus the absorption of neutral pions in the interaction

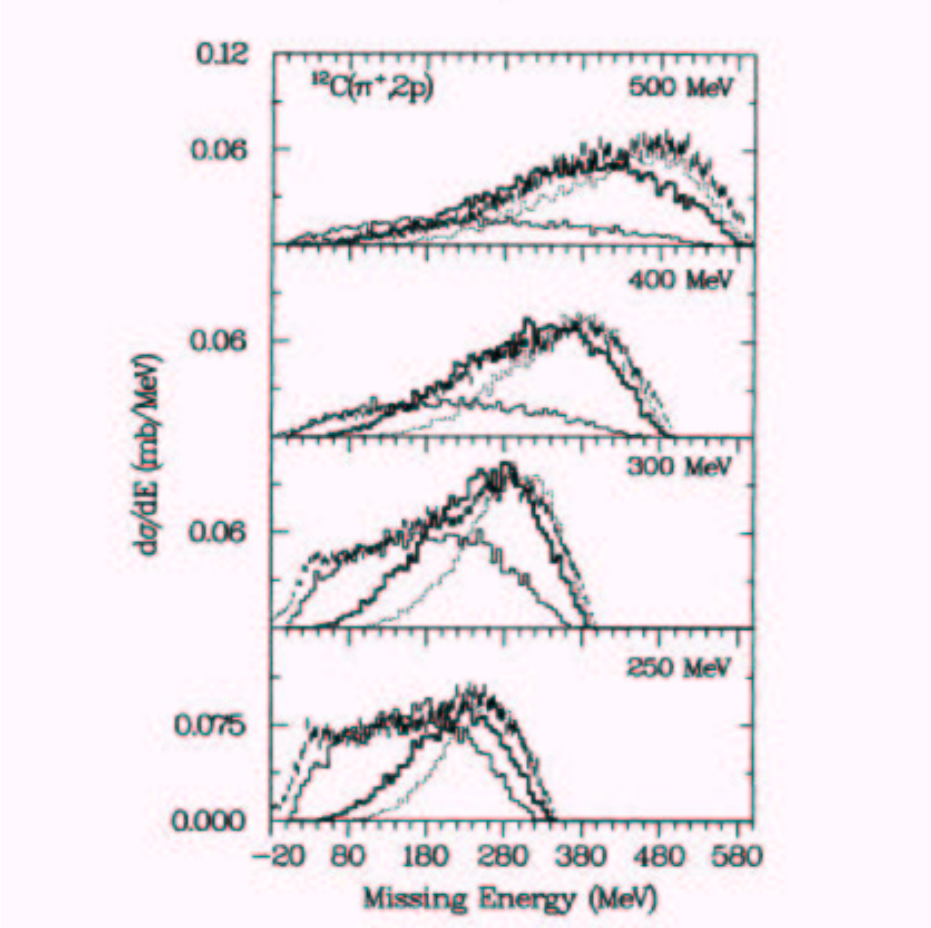

Figure 8: The missing energy (total pion energy minus the total proton kinetic energy) for the absorption of 250-500 MeV pions on carbon.

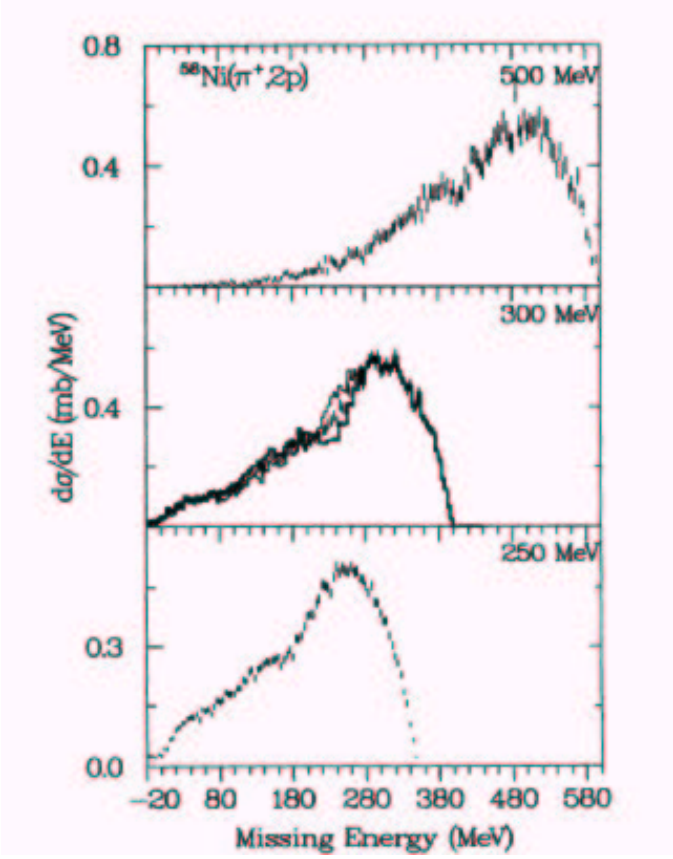

Figure 9: The missing energy (total pion energy minus the total proton kinetic energy) for the absorption of 250-500 MeV pions on nickel.

nucleus must also be taken into account in any study of resonance production.

We have begun studies with INTRANUKE to determine the sensitivity to the probability of pion absorption in the interaction nucleus. We are currently in the process of modifying Monte Carlo routines to treat pion absorption more realistically. Because MINERνA will also have good neutron detection capability, we expect to be able to substantially improve the determination of the incident neutrino energy.

We also wish to note that there are essentially no measurements of pion absorption above 500 MeV. The fine spatial resolution and full solid angle detection capability of MINERνA will allow us to study these interactions, especially in carbon.

4.2 Nuclear Transparency in Neutrino Interactions

A second nuclear interaction process which affects the observed final state energy is the final state interaction of a nucleon in the struck nucleus. An outgoing nucleon has a substantial probability of interacting in the nucleus. These probabilities have been measured, most recently at JLab, with some precision. The experiments used $(e, e'p)$ coincidence reactions. The cross section for finding the scattered electron in the quasi-elastic peak was compared to the cross section for finding the coincident proton. A summary of the results are shown in Fig. 10.

In contrast to pion absorption, there is little available information on what happens to the scattered nucleon. Of course, most either scatter from a single nucleon quasi-elastically or produce a pion (for protons above 600 MeV). Improving Monte Carlo routines to model this interaction should allow us to better estimate the total final state energy. As with pion absorption, the good resolution, neutron detection capability, and full solid angle coverage of MINERνA should allow us to experimentally determine the actual final states and constrain the Monte Carlo routines.

4.3 Proposed Experimental Analysis

The NEUGEN Monte Carlo has been used to study the sensitivity of the MINERνA experiment to nuclear effects. The nuclear effects in the NEUGEN Monte Carlo are controlled by the INTRANUKE processor. This processor incorporates a probability for pion absorption based on earlier eletroproduction absorption studies and lower-statistics Ne/H_2 neutrino bubble chamber data. The observed phenomena of hadron formation length, which increases the transparency, is incorpo-

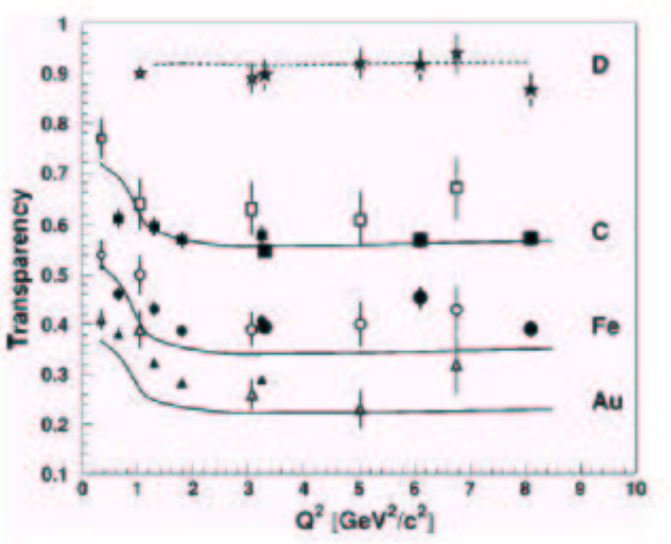

Figure 10: Probability for the outgoing proton to escape the nucleus as a function of Q^2.

rated as well. The particular model used for pion absorption, which is currently being improved and updated, assumes that the absorption process eliminates a pion and the resulting nucleons are themselves either absorbed in the nucleus or are too low in energy to be observed in the detector.

To determine the sensitivity of MINERνA measurements to the predictions of this model, the assumed probability for pion absorption in INTRANUKE has been increased by three standard deviations and then decreased by the same amount. The multiplicity and a very crude estimate of the visible hadron energy have been examined under these extreme conditions. In the next series of figures the predicted asymmetry in the multiplicity and visible hadron energy are shown. Currently we have only a very small sample of 2500 generated events available for this analysis. The asymmetry is defined as the percentage change under these extreme assumptions. That is, the bin contents at plus three standard deviations minus the bin contents at minus three standard divided by bin contents at minus three standard deviations. Figure 11 shows the predicted change in the multiplicity distributions for carbon, while Figure 12 shows the same distribution for iron. Both figures are consistent with the model that the decrease in observed multiplicity is caused by an increase in absorption probability and therefore the effect should be stronger in Fe than in C. The final determination of the visible hadron energy will

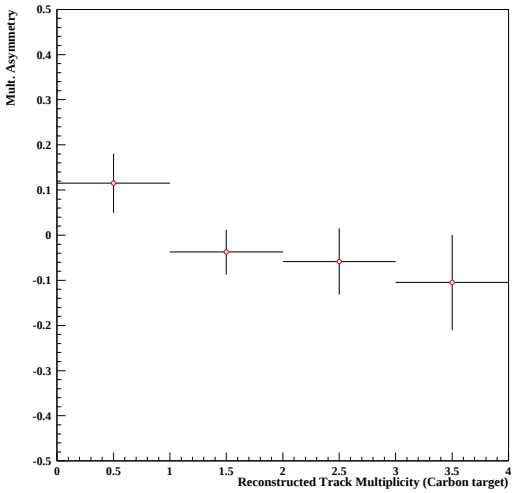

Figure 11: The fractional change in multiplicity distributions between the two values assumed for pion absorption on carbon described in the text.

be an involved process for this experiment. For now, we are using the most primitive estimate of this quantity, namely an uncorrected version derived from the total light output of the hadron shower. In the data analysis this will be refined for example, through measurements of stopping/decaying particles. With this crude estimate, the change in hadron energy for iron is shown in Figure 13 and for lead and Figure 14. There is a dramatic change, even with these low simulation statistics, in the lowest energy bin. MINERνA will collect several times these statistics and should be capable of measuring this effect at even higher hadron energy.

Since the incoming neutrino energy is not *a priori* known, the measured **muon** kinematics will be tested as a basis to compare characteristics of the visible hadron shower across nuclear targets and to determine whether the nuclear-effects correction-factor is a function of the observed muon kinematics. The muon is relatively free from nuclear dependent effects and serves well as an A-independent normalization. For example, the quantity:

$$Q' = 4E_{\mu}sin^2(\theta/2) \tag{2}$$

is representative of the square of the 4-momentum transfer to the nucleon or quark, weighted (inversely) by E_{ν}. This quantity then reflects the energy-momentum transferred to the hadronic vertex. The distribution of events in this quantity are peaked toward low Q' with half the events below Q' = 1.0. The Monte Carlo statis-

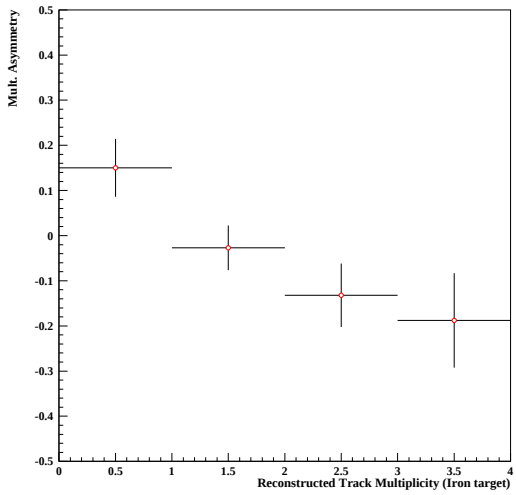

Figure 12: The fractional change in multiplicity distributions between the two values assumed for pion absorption on iron discussed in the text.

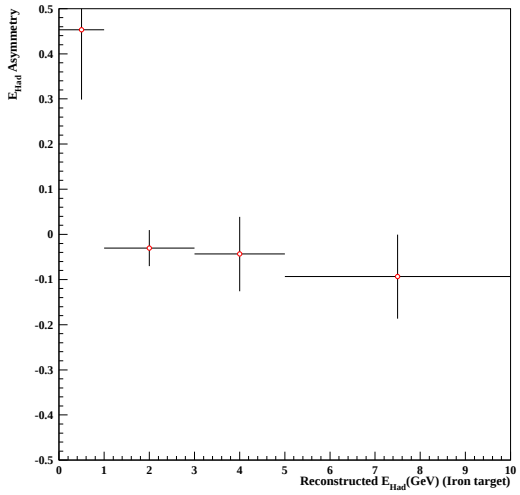

Figure 13: The fractional change in the visible hadron energy distributions between the two values of pion absorption on iron discussed in the text.

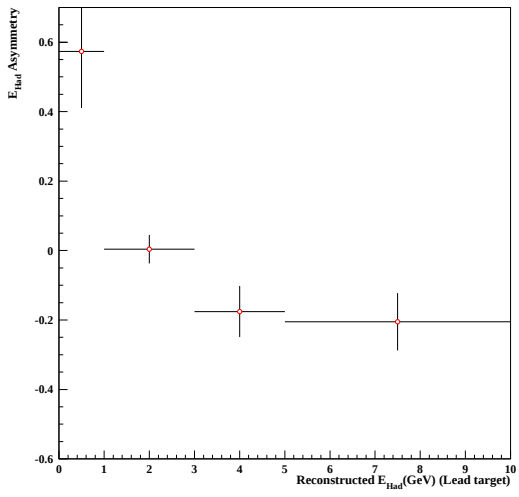

Figure 14: The fractional change in the visible hadron energy distributions between the two extremes in pion absorption on lead discussed in the text.

tics are still too low to make any conclusions on this study at this point, however the trend is encouraging and the study will continue with increased statistics.

5 Resonance Production at MINERνA

Resonance production is an important issue both for future oscillation experiments, where resonant final states comprise much of both the signal and backgrounds, and for MINERνA itself where the comparison of resonance production in electron and neutrino scattering provides an important motivation for our physics program in the low energy beam at NuMI. For the latter studies, a joint effort has been launched between the neutrino and electron communities to better utilize the available electron scattering data for improved neutrino cross section modeling, considering nuclear effects as well as production mechanisms. This collaboration was recently approved by the Jefferson Lab Program Advisory Committee to measure low Q^2, separated structure functions in the resonance region on a variety of targets of interest to the neutrino community (JLab Hall C Experiment E04-001). Many details of the MINERνA program in resonance production are given in the proposal[5].

Broadly, the resonance production measurements will focus on two areas. Fundamentally, MINERνA will measure pion production cross sections on a variety of nuclear targets nuclear targets, carbon and heavier. Secondly, the understanding of nuclear effects gained from these measurements will allow us to "extrapolate" the measurements to the free nucleon. Comparing these measurements to electron scattering will allow a better understanding of the axial component of neutrino resonance production. As nuclear effects will be important in all the measurements, we review below approaches to understanding the nuclear effects. This is followed by a discussion of ongoing studies of event and particle identification techniques relevant to single pion production.

5.0.1 Nuclear Corrections

The interaction of neutrinos in nuclei produce secondary particles which propagate though the nucleus. Among them are protons produced in quasi-elastic scattering and pions produced in the resonance region. These effects are usually accounted for in Monte Carlo programs, such as the MINERνA simulation, and in an analytic method described here.

The propagation is viewed as a two step process:

- A proton (QE) or a pion is produced on a bound proton or neutron, corrected for Pauli blocking and Fermi motion.

[5] see chapters 7, 10 and 13 of the MINERνA proposal [1]

- The produced particle propagates through the nucleus performing a random walk and it may exchange its charge in each interaction.

The assumptions allow a general description of the problem based on charge symmetry and isospin conservation. The main property is a factorization of production and subsequent propagation. For the produced pions for instance we can write,

$$\begin{array}{c} N_f(\pi^+) \\ N_f(\pi^0) \\ N_f(\pi^-) \end{array} = M \left(\begin{array}{c} N_i(\pi^+) \\ N_i(\pi^0) \\ N_i(\pi^-) \end{array} \right) \tag{3}$$

where the subcript i denotes the number of pions produced initially at the neutrino interaction and, similarly, the subscript f denotes the number of pions emerging from the nucleus. The matrix M has a special form, which follows from isospin symmetry.

$$\frac{M}{A} = \left(\begin{array}{ccc} 1-c-d & d & c \\ d & 1-2d & d \\ c & d & 1-c-d \end{array} \right) \tag{4}$$

The parameter A contains absorption of the pion and the Pauli blocking in the pion interactions. The parameters c and d involve the effects of charge exchange in the re-scattering. The formalism can be used in two ways:

- To observe the yields in a specific nucleus and compare them to production of pions on free protons and neutrons. Simple algebra relates the parameters to the observations. Thus determining the parameters in electroproduction allows one to use them in charge and neutral current neutrino reactions.

- To calculate A, c and d theoretically by solving the random walk problem. The numbers produced by the two methods are compatible with each other.

More results are expected from the present experiments and MINERνA will contribute on this topic. The method is needed to interpret the data and to determine oscillation parameters.

As an illustration, we show in Figure 15, the yields of pions in electroproduction and neutrino experiments on an ^{16}O target. The curves in the upper graph show the yields for π^0s. The dotted curve shows the production on free isoscalar target,i.e. $1/2(n+p)$. The solid curve shows the reduction produced on an oxygen target, where the change is substantial. The lower graph shows yields of π^+s where the nuclear corrections are much smaller.

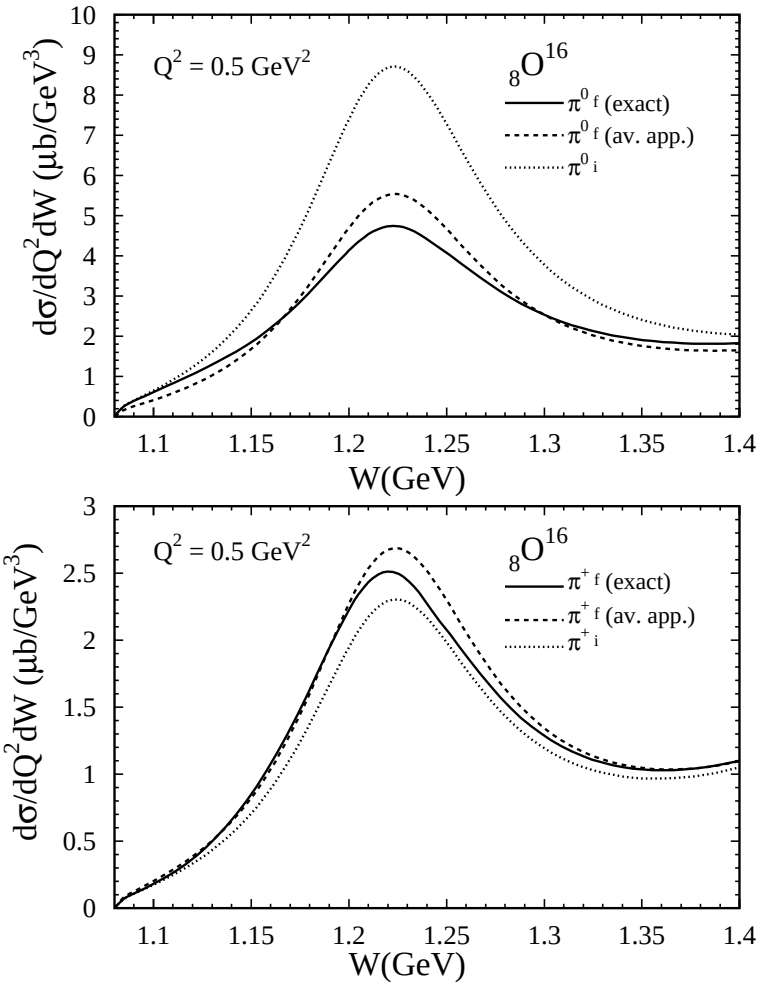

Figure 15: Dotted lines show electroproduction cross sections for π^0 and π^+ on an ^{16}O target, with no final state interactions. The solid curves show these cross sections after the nuclear effects of pion re-scattering and absorption, according to the model of Paschos et.al.[] The final state interactions greatly attenuate the π^0 yield. However, charge exchange from the larger π^0 production cross section serves to roughly balance the losses for the π^+ channel, keeping the the π^+ yield about the same before and after pion reinteractions. Except for the overall scale of the cross section, these same results are predicted for neutrino neutral current reactions.

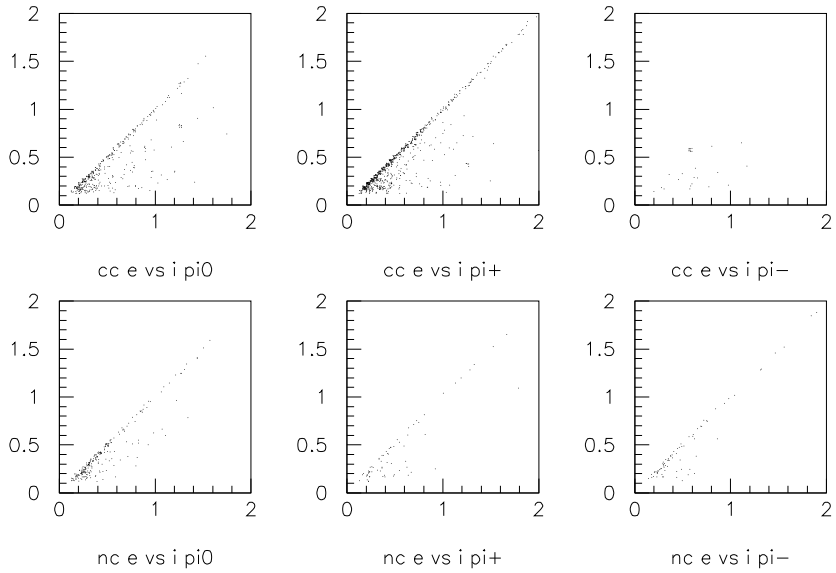

Figure 16: Correlation of pion energies before and after intranuclear re-scattering as implement in NEUGEN for the MINERνA simulation. Events are generated within the central plastic region (carbon and hydrogen scatterers) of the detector. Each plot shows on the vertical axis, the pion energy after it exits the nucleus versus the energy at the point that it is produced inside the nucleus. The first row of figures if for CC interactions while the second if for NC scattering. The left column is neutral pions, while the middle and right columns are for positive and negative pions. Pions that do not re-scatter in the nucleus fall along a diagonal line, while re-scattered pions fall below the line. These correlations indicate that while re-scattering is important, pions exiting the nucleus will still carry information about their initial state. The top right figure shows the correlation for negative pions arising from CC scattering. Production of single negative pions is forbidden due charge conservation, so negative pions will only be created by charge exchange from neutral pions.

The MINERνA monte carlo simulation, which uses the NEUGEN neutrino event generator also includes a type of random-walk simulation of pion re-interactions. These pion re-scatterings are implemented using the INTRANUKE [11] pion cascade model. With this model, the correlation of pion momenta before and after final state interactions can be studied. For $^{12}\mathrm{C}$, (Figure 16), while some pions do scatter and loose momentum, many retain their original momentum. This correlation suggests that pion production data on carbon will be able to constrain free nucleon resonance production cross sections. While these correlations are not observable, MINERνA will be able to test the pion re-scattering models by studying the A dependence of pion yields and distributions.

5.1 Event Identification and Particle ID

In electron scattering, resonance excitation spectra can be measured by detecting just the electron. However, in neutrino scattering, W and Q^2 must be reconstructed using energies of the final state hadrons. Since the proposal, we have begun a program of studying resonance reconstruction in the MINERνA detector using using our hit-level Monte Carlo simulation and the NEUGEN neutrino event generator. The techniques initially being studied are topological cuts to identify overall reaction type, and particle identification of individual tracks.

We have performed a first analysis of single pion production detection efficiencies using simple topological cuts. The event selection here is very simple; tracks in the fully active target pointing to the vertex are counted and are identified as charged or neutral by the distance between the vertex and the first hit of a track. Tracks with a first hit less than 5 cm from the vertex are labeled as charged, while tracks further from the vertex are labeled as neutral (photons from π^0 decay or neutrons).

With these simple track multiplicity and vertex cuts, for example, $\mu^- p \pi^\pm$ events are identified with over a 90% efficiency nearly independent of pion energy. Background processes comprise less than 2% of events passing this two charged track cut even without particle identification cuts. Events with neutral pions are also identified with good efficiency with these cuts. For example, a topological cut designed to isolate a sample of neutral pions accompanied by zero or one nucleons and zero or one muons, such as the $\mu^- p \pi^0$ event illustrated in Figure 17, results in identification of a sample containing 75% of single neutral pion resonance events with only 10% background. This is in the absence of particle identification requirements on the π^0, such as invariant mass reconstruction

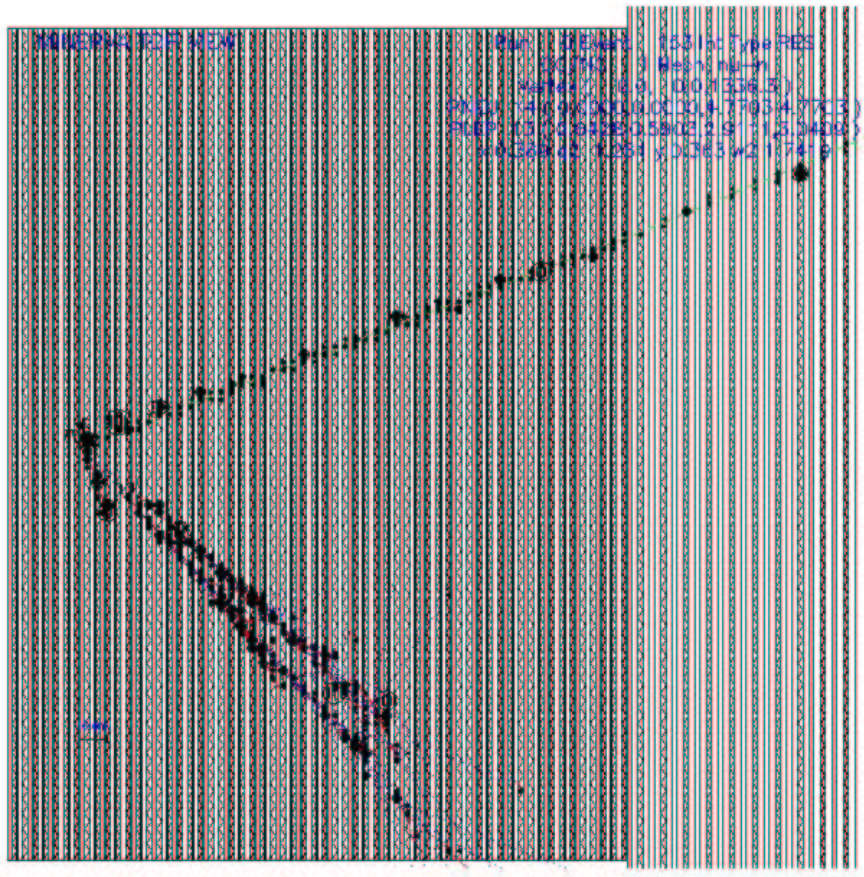

Figure 17: Event display example of charged current event with a muon, proton and neutral pion. This event passes a simple topological selection of π^0 events. The proton has hits close to the vertex, while the π^0 photons convert well away from the vertex.

techniques that are described in the MINERνA proposal[6].

For charged pions, this topological analysis depends on detecting a nucleon with the pion, which biases against pions with low momentum nucleons. Since the full tracking will likely be able to distinguish pions by dE/dx, particularly for low energy pions, it should be possible to produce inclusive energy and angle spectra of single pions that can be compared directly against pion re-scattering models such as Paschos, et.al., described above, or the pion nuclear cascade models in neutrino event generators. The shapes of initial and re-scattered pion spectra predicted by NEUGEN are shown in Figure 18. Additional capabilities in particle identification, such as identifying production of pions in "forbidden charge" states, e.g., $\mu^- p \pi -$, will provide a check of pion reinteraction models as these can not arise from single pion production on a nucleon through the charged current reaction. Understanding these reinteractions is ultimately very important for oscillation analysis as it is these reinteractions that limit the ability to transfer knowledge of resonance production from charged lepton data to neutrino scattering.

In addition to identification of resonance production events by simple vertex topology, particle identification will be required to differentiate the proton and charged pion in a $p\pi^{\pm}$ final state, and possibly identify pion charge. As described in the proposal, particle identification in MINERνA will rely on measuring discriminating particle characteristics, such as specific energy loss (dE/dx) as well as topology (hadron and electromagnetic showers, decay signatures). As noted above, photons will appear as showers disconnected from the vertex, and π^0 will appear as two photons pointing back to the vertex, with invariant mass consistent with the π^0 mass.

Of particular consideration are low energy particles that stop in the target area without entering the magnetic field. We have already demonstrated in the proposal our ability to separate $\pi^{\pm}$ from $K^{\pm}$ and protons. However, we would like to be able to distinguish π^+ from π^- in the inner tracker alone. Indeed, there are physics processes visible in the highly segmented low density target can allow such separation. Shown in Figure 19 is the display of a neutrino interaction in the target area before GEANT digitization. A muon (red), proton (blue), π^+ (green) that decays in a $\pi \rightarrow \mu \rightarrow e$ sequence (green-magenta, the muon is not seen). However, a π^- (black) scatters before stopping without visible interaction or may charge exchange with nuclei in the target to produce a neutral pion.

In order to study the π^+/π^- differences we generated pion interactions at 0.1,

[6]see Sections 8.3 and 13.6.2 of the MINERνA proposal [1]

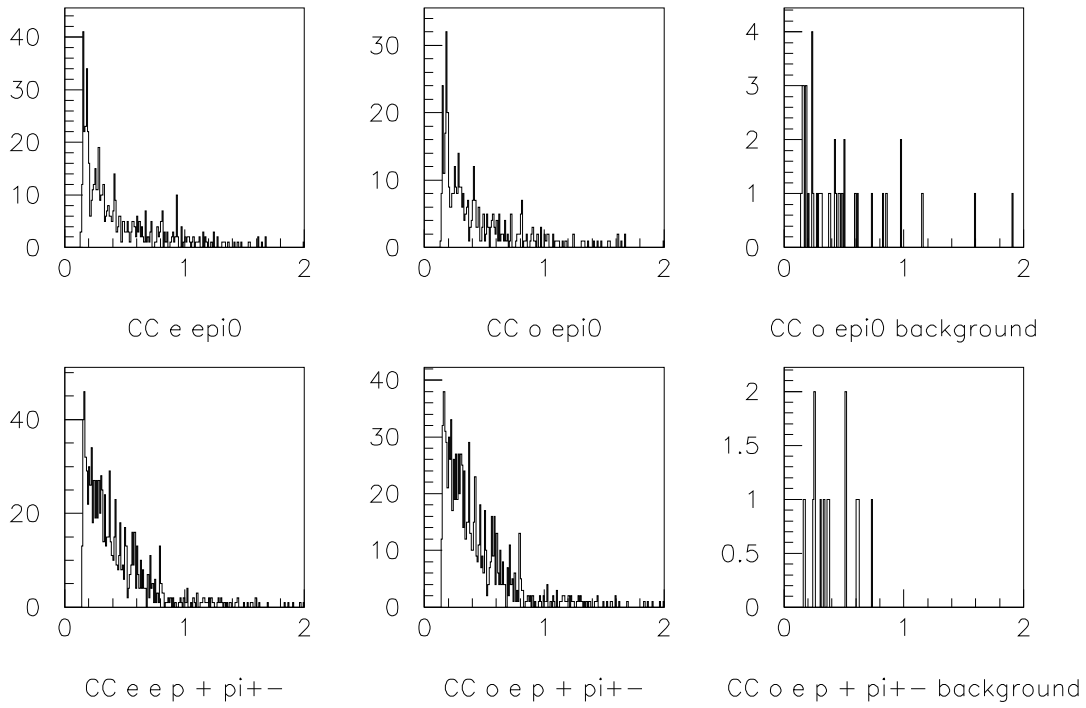

Figure 18: The top row shows pion energy distributions for events that contain a single π^0 and zero or one nucleons, while the bottom row is of events with a single charged pion (positive or negative) and a single proton. The left column shows the distributions using known/truth particle identification from the monte carlo. The second and third column are events that have been identified using the simple topological cuts discussed in the text. The middle column is events that have been correctly identified, while the right column is events of other types that have been misidentified as the respective single pion event types. The simple cuts correctly identify about 75% of the π^0 events, admitting about a 10% back from other types of events. The charged pion efficiency is about 95% with less than 2% contamination of background events. Within the statistics of this sample, the efficiencies of event type identification are independent of pion energy.

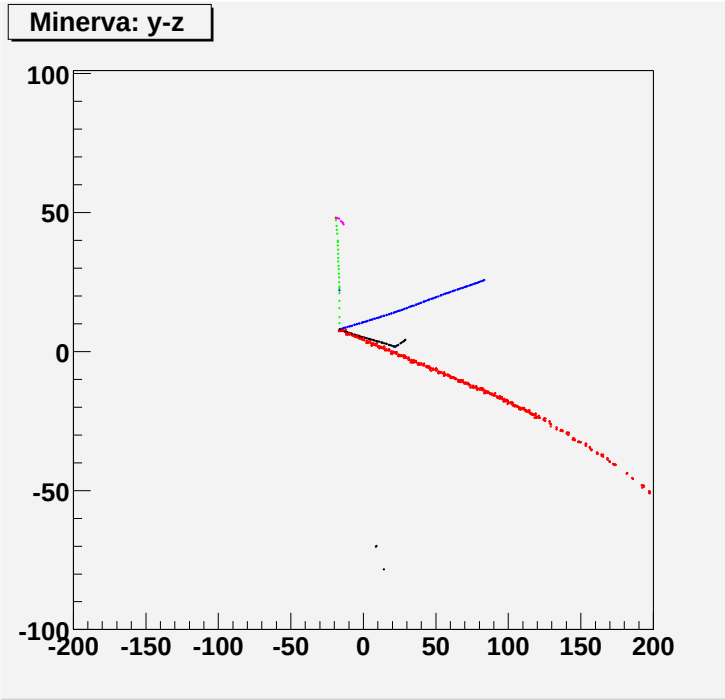

Figure 19: A π^+ Decay Chain in MINERνA

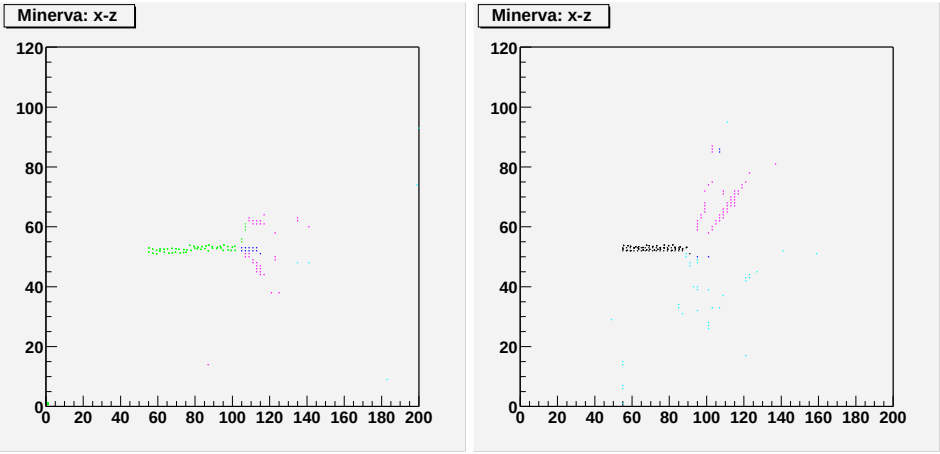

Figure 20: π^+ and π^- Interactions in MINERνA

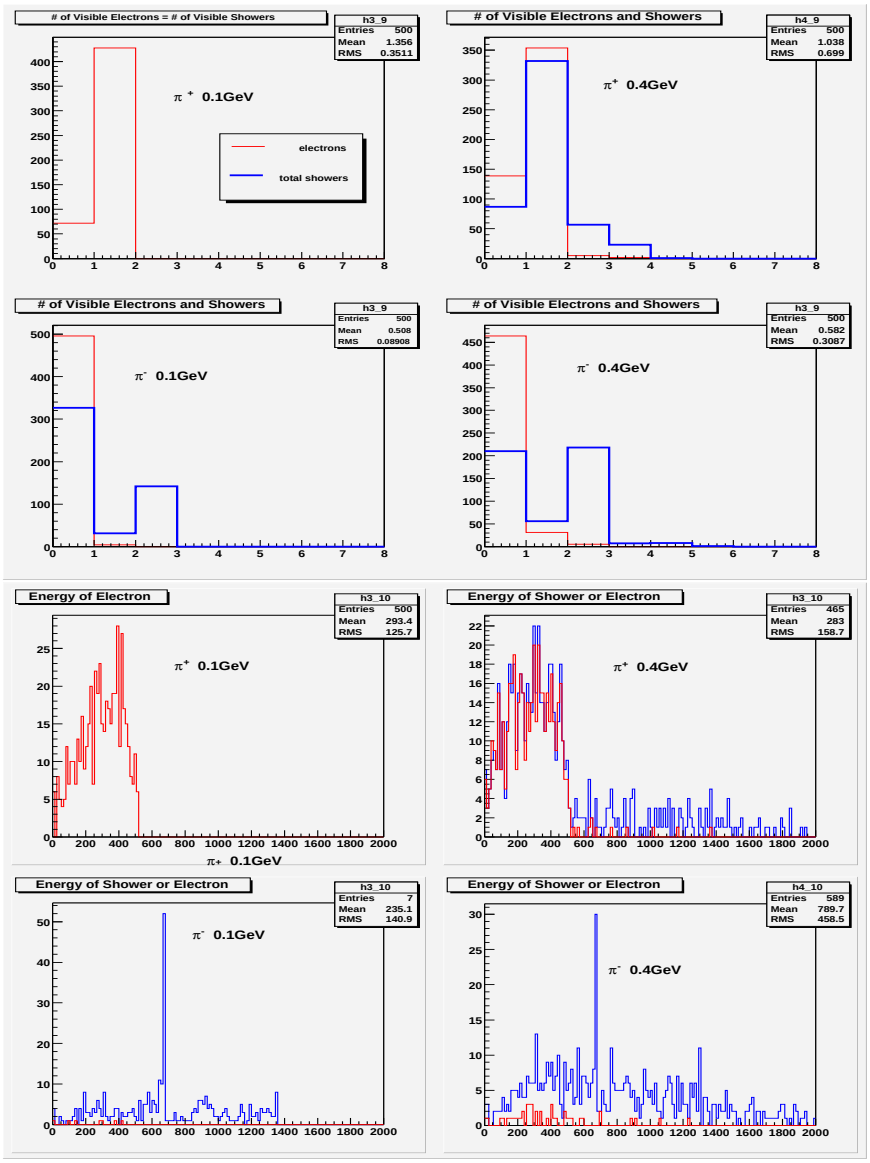

Figure 21: Electron shower multiplicity and energies for π^+ and π^- Interactions in MINERνA

0.4, 0.8, and 1 GeV/c in our target using the MINERνA simulation. As a case study, the two interactions in Figure 20, show a 1 GeV/c π^+ in MINERνA. The final π^+ decays ($\pi \rightarrow \mu \rightarrow e$) with the muon not seen, but with a clear positron (magenta). A proton (blue) is also seen coming out of the vertex as well as two gammas (magenta) pointing to the vertex. The $\pi \rightarrow \mu \rightarrow e$ sequence is characteristic to all stopping π^+. In the second interaction, we see a π^- interaction with charge exchange $\pi^- p \rightarrow \pi^0 n$ as seen in the central detector (after GEANT digitization). The characteristic π^0 (two showers magenta) accompanies low energy π^-. These differences in final state can be observed by studying the electron shower multiplicity and energy associated with charged π tracks as shown in Figure 21. We conclude that although these issues need still more study that the MINERνA inner tracker is capable of statistical $\pi^{\pm}$ separation even without a magnetic field.

6 MINERνA and Oscillation Measurements

Examples of oscillation measurements that will benefit from MINERνA are the Δm^2 determination by MINOS, and the $\nu_\mu \rightarrow \nu_e$ oscillation probability measurement by the NuMI Off-axis ν_e Appearance (NOνA) and the T2K experiments. In chapter 13 of the proposal we presented an estimate for how much uncertainties in nuclear effects would contribute to uncertainty in Δm^2 in MINOS; here we update that estimate with an improved treatment of nuclear effects, and consider two consequences of these effects separately. After discussing the Δm^2 measurement we then describe how NOνA can utilize MINERνA measurements of cross sections to minimize the systematic error on its oscillation probability measurement. In the proposal we described the challenge of measuring the $\nu_\mu \rightarrow \nu_e$ oscillation probability due to the uncertainty in backgrounds that must be rejected at a high level, and improvements that MINERνA can provide to neutrino event generators that will used to predict those backgrounds. We present here a new analysis (which is also part of the NOνA proposal, chapter 9) which shows quantitatively how uncertainties in cross sections translate to uncertainties in background predictions. We also show that information MINERνA provides will be important regardless of the size of oscillations that NOνA observes. If NOνA sees no evidence for ν_e appearance then MINERνA's most important contribution will be to improve the determination of the background at the far detector. However, if NOνA does see a signal, then the reduction of the cross section uncertainties plays an even larger role in helping NOνA achieve the best precision on its measurement of the $\nu_\mu \rightarrow \nu_e$ oscillation probability.

6.1 Nuclear Effects and a Δm^2 measurement

The key to a precise measurement of Δm^2 is the ability to measure the oscillation probability as a function of neutrino energy. Although MINOS has undergone an extensive program to determine the response of its near and far detectors to specific charged particles, it cannot measure the likelihood with which those particles are produced in a neutrino interaction. At these low neutrino energies, there are two effects that become important, and therefore contribute significantly to the uncertainty in a measurement of Δm^2. One effect, which is independent of the target nucleus, results from the rest masses of the secondary particles which contribute an important fraction to the reconstructed neutrino energy. A measurement of final state particle multiplicities and species as a function of hadron energy, which cannot be measured in MINOS, is therefore important for accurate recon-

struction of the neutrino energy spectra at both MINOS detectors. Secondly, as shown in the proposal, the multiplicity distribution is a function of target nucleus, since secondary particles can either scatter in the nucleus, or be completely absorbed. Either process results in a change in the visible hadron energy for an event, again contributing to the uncertainty in the measurement of the neutrino energy spectrum.

Figure 22 shows the changes in the ratio of visible to total neutrino energy for uncertainties in absorption (top) and scattering (bottom) separately. In the proposal these two effects were not shown separately. Furthermore, nuclear effects were assumed to be the same for carbon as for steel, and a flat 20% uncertainty on the nuclear plus rest mass effect was assumed. The visible energy is defined as the sum of the kinetic energies of all the charged final state particles, plus the total energy for the neutral pions, (since it is assumed they deposit all their energy in the form of electromagnetic showers). In the top plot, for a steel target, the parameter in the event generator that describes pion absorption is varied by three standard deviations. In the bottom plot pion absorption is turned off, and the visible energy to total energy ratio is compared for steel, carbon, and lead. Figure 23 shows the effect of changing the pion absorption on the visible neutrino energy spectra for both near and far detectors (with Δm^2 is $2.5 \times 10^{-3} eV^2$). The effect is also shown (Figure 23 bottom) as a ratio for both the near and far spectra as well as the effect of the change on the far/near ratio. It is clear that although the visible energy difference produces the same kind of effect in near and far spectra, it only partially cancels because of the different underlying neutrino spectra.

Evaluating the appropriate uncertainty in the size of nuclear effects in neutrino scattering is non-trivial, because the only precise data on differences between nuclei come from charged lepton scattering, and one has to use theoretical models to translate the effects from the charged leptons to the neutral leptons. The "three standard deviations" in pion scattering were measured in a bubble chamber experiment, not on steel, therefore, a theoretical extrapolation must be made for the target in this case. If we naively take the differences described above as "one standard deviation" for pion absorption, and the differences between steel and carbon or lead as "one standard deviation" for pion rescattering, we can determine how this systematic error would compare to the MINOS statistical error. The top plot in Figure 24 shows how raising and lowering pion absorption would lower and raise, respectively, the measured Δm^2. The central plot shows how assuming nuclear effects for lead or carbon, compared to steel, would again lower or raise, respectively, the measured Δm^2. The bottom plot in Figure 24 shows the two sets of errors added in quadrature.

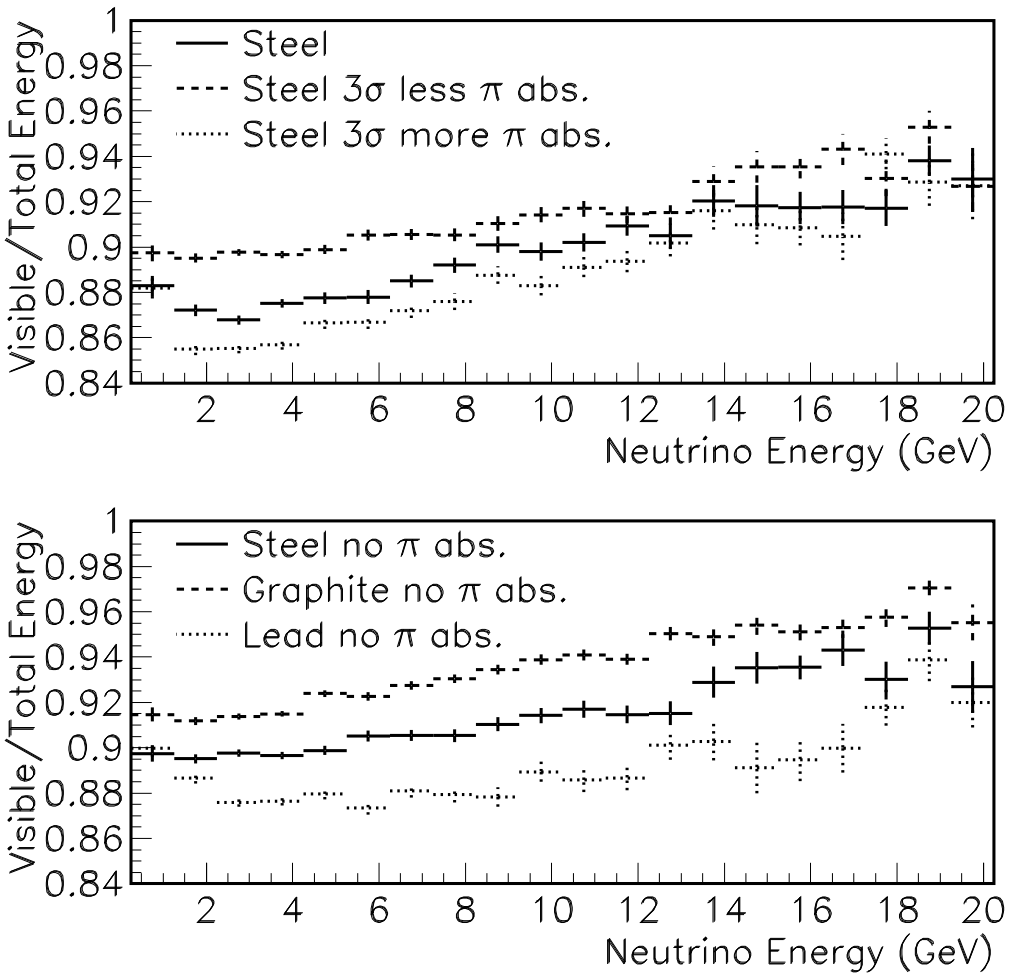

Figure 22: Ratio of visible to true neutrino energy for several different models of nuclear effects. The top plot shows the ratio for steel (solid) with the nominal pion absorption, as well as the same ratio for the pion absorption cross section varied by plus and minus three standard deviations. The bottom plot shows the differences in the average of this ratio for three different target nuclei, where the absorption effects are turned off to see more clearly the effects of pion rescattering.

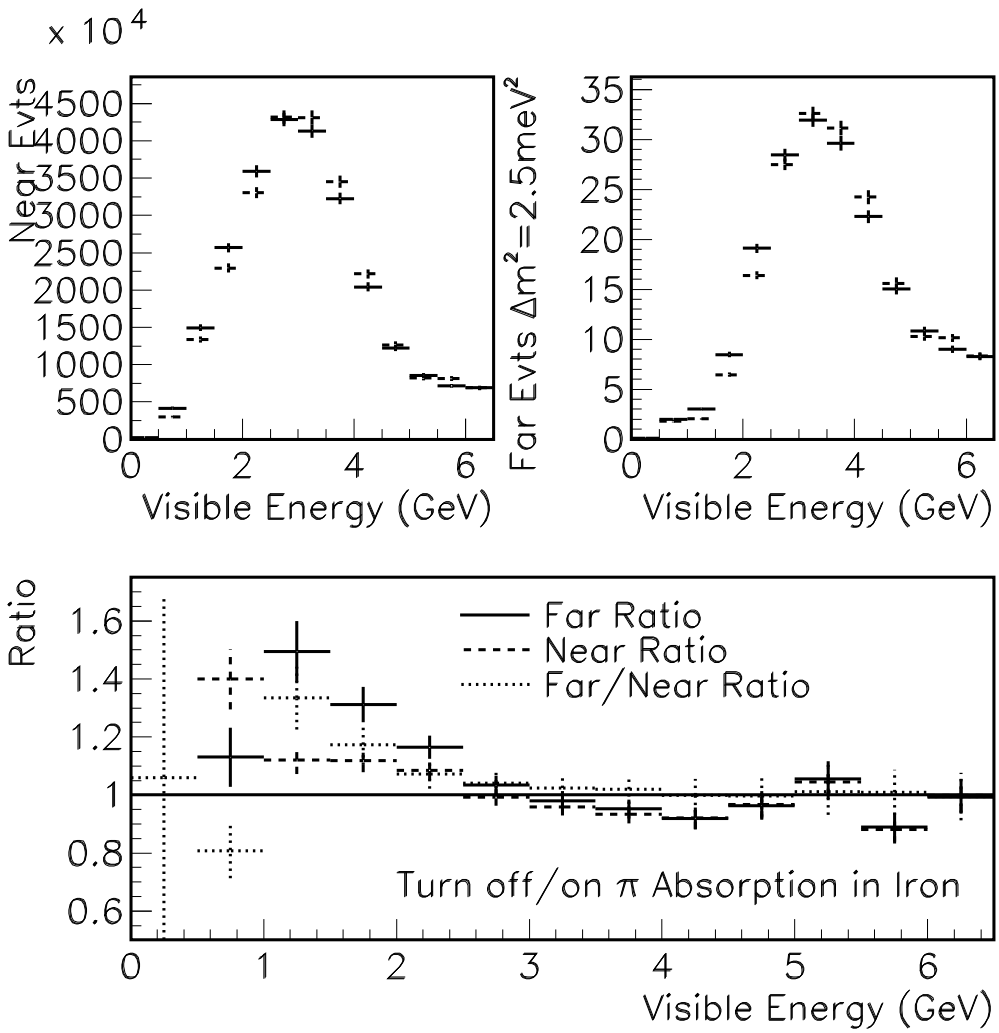

Figure 23: **(Top left)** visible neutrino energy spectrum for the near detector for ν_μ CC events, for nominal and three sigma high pion absorption in iron. **(Top right)** visible neutrino energy spectrum for the far detector for ν_μ CC events, again for nominal and three sigma high pion absorption. Δm^2 in this case is assumed to be $2.5 \times 10^{-3} eV^2$. **(Bottom)** Ratio of changed divided by nominal pion absorption model, for the far (solid) and near (dashed) energy spectra, as well as the ratio of far over near. Note that the effect of pion absorption cancels somewhat in the ratio of far over near event spectra, but not completely.

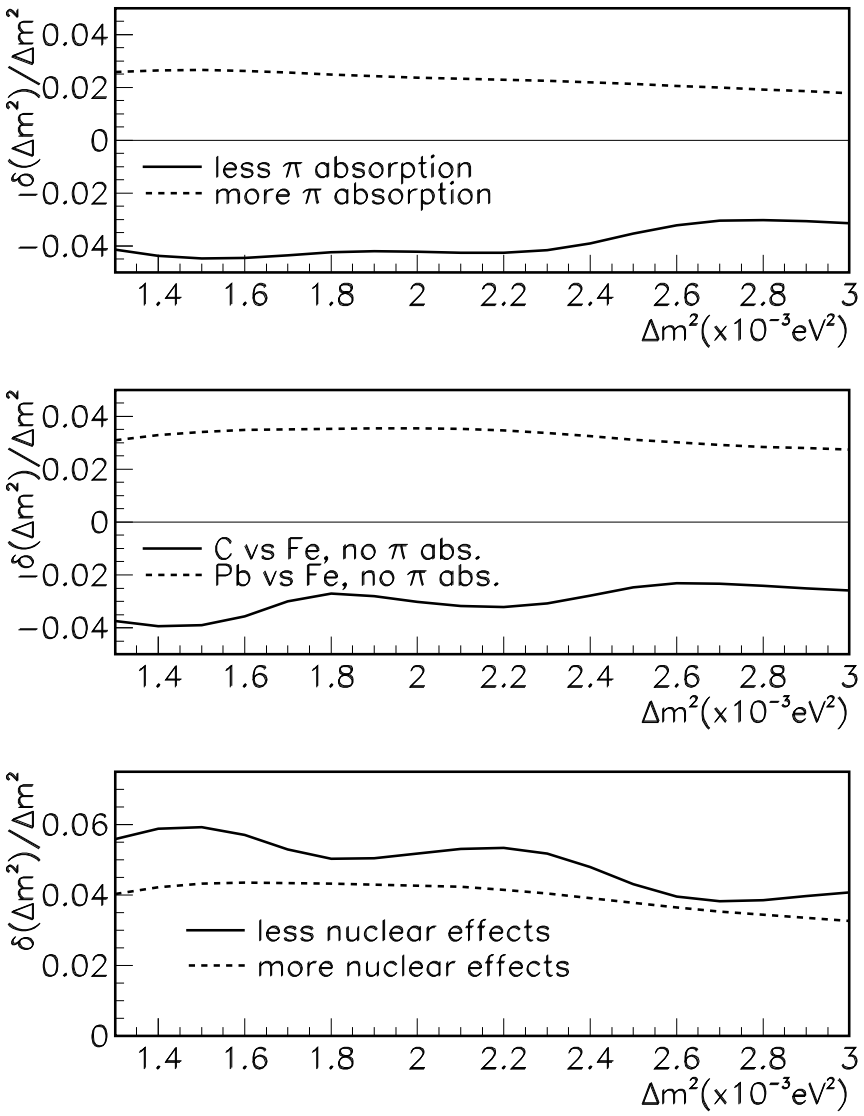

Figure 24: **(Top)** Increase (decrease) in the measured Δm^2 due to a decrease (increase) in the pion absorption cross section on Iron. Middle plot: Increase (decrease) in the measured Δm^2 due to assuming the target had the nuclear effects of Carbon (Lead) compared to Steel, when pion absorption is turned off. **(Bottom)** The errors due to increases (decreases) in Δm^2, added in quadrature, as a function of Δm^2.

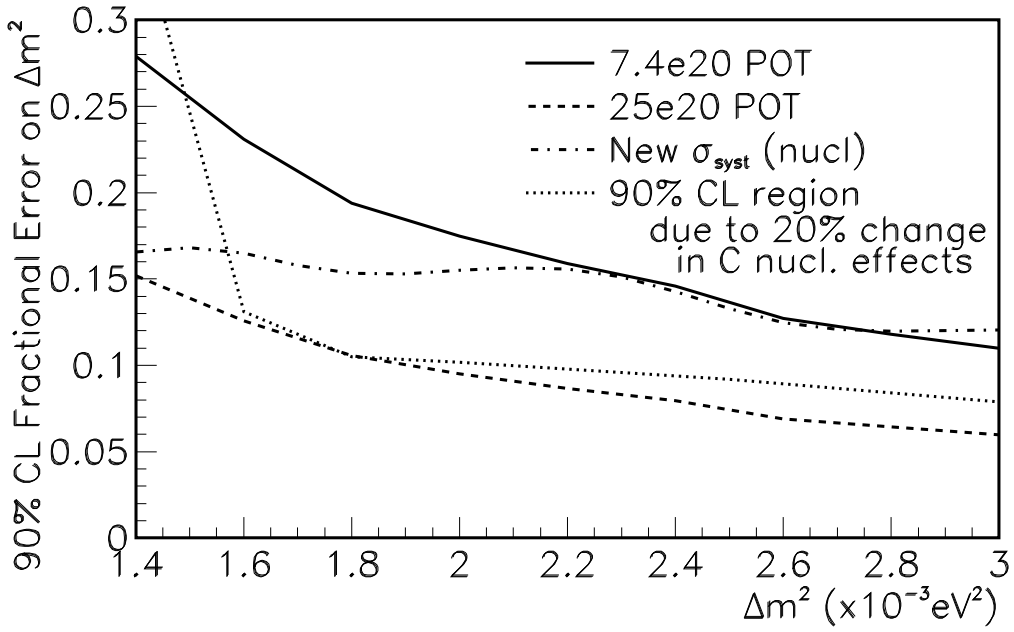

Figure 25: Fractional size of the 90% confidence level region at $\sin^2 2\theta_{23} = 1$ for the changes in nuclear effects described earlier, assuming the uncertainties for nuclear effects in neutrinos are three times the uncertainties coming from the charged lepton measurements.

If these errors are appropriate, then they are comparable with the statistical error expected by MINOS for 7.6×10^{20} protons on target, as shown in figure 25. Also shown on this plot is the previous uncertainty that was shown in the proposal, which was evaluated assuming the nuclear effects were known to 20%, and which assumed the size of nuclear effects on carbon were the same as those on steel. As described in the section on nuclear effects in this addendum, MINERνA will be able to measure these effects in neutrino scattering directly and precisely, for several different targets.

6.2 Measurements of $\nu_\mu \rightarrow \nu_e$ oscillation Probability

In order to understand the full importance of MINERνA cross section measurements for the NOνA experiment, it is helpful to revisit how experiments will determine the $\nu_\mu \rightarrow \nu_e$ oscillation probabilities. The number of events in the far detector can be described as

$$N_{far} = \phi_\mu P(\nu_\mu \rightarrow \nu_e)\sigma_e \epsilon_e M_{far} + B_f \tag{5}$$

Where ϕ_μ is the muon neutrino flux at the far detector, P is the oscillation probability, σ_e and ϵ_e are the electron neutrino cross section and efficiency, respectively, and M_{far} is the far detector mass. The backgrounds at the far detector, B_{far}, can be expressed as

$$B_{far} = \Sigma_{i=e,\mu}\phi_i P(\nu_i \rightarrow \nu_i)\sigma_i \epsilon_i M_{far} \tag{6}$$

Where the notation is the same as equation 5, but ϵ_i is the efficiency for a neutrino of type i to be misreconstructed as an electron neutrino. Backgrounds come from both muon and electron neutrinos, and from several different neutrino interaction channels. Both equation 5 and 6 must be summed over neutrino channels, as well as integrals over neutrino energy.

The error on the oscillation probability, in this simplified notation, can then be expressed as

$$\frac{\delta P}{P} = \frac{N_{far} + (\delta B_{far})^2}{(\phi_\mu \sigma_e \epsilon_e M_{far})^2} + (N_{far} - B_{far}) \left[(\frac{d\phi}{\phi})^2 + (\frac{\delta\sigma}{\sigma})^2 + (\frac{\delta\epsilon}{\epsilon})^2 \right] \tag{7}$$

The two terms in equation 7 suggest two regimes: in the case where the number of events in the far detector is comparable to the background prediction, the

Process	Statistics	QE	RES	COH	DIS
$\delta\sigma/\sigma$		20%	40%	100%	20%
Signal ν_e	175 ($\sin^2 2\theta_{13} = 0.1$)	55%	35%	n/I	10%
NC	15.4	0	50%	20%	30%
$\nu_\mu CC$	3.6	0	65%	n/I	35%
Beamν_e	19.1	50%	40%	n/I	10%

Table 3: List of the signal and background processes than can contribute events in the NOνA far detector, for a 50kton detector located 12km from the NuMI axis, 820km from Fermilab, assuming a Δm^2 of $2.5 \times 10^{-3} eV^2$. Also given are the cross section uncertainties on those processes before MINERνA runs.

error on the probability is dominated by a combination of statistics and the uncertainty on the background prediction. The background prediction uncertainty is dominated by the uncertainty in the background process cross sections and efficiencies. In the other extreme, where the number of events is dominated by the signal events, the uncertainty on the probability comes from the statistics, and the uncertainties on the signal channel cross sections and efficiencies.

For the NOνA detector simulation running at an off axis location 12km from the NuMI beamline and 820km from the source at Fermilab, the signal and background statistics for the nominal 5 year run are given in table 3. As has been described in more detail in both the NOνA and MINERνA proposals, the three categories of backgrounds are ν_e's originally produced in the neutrino beam, the neutral current events with energetic neutral pions which can fake electrons, and ν_μ charged current events, where the final state muon is low energy and the event contains a high energy neutral pion. Also given in Table 3 are the fractions that each neutrino interaction process contributes to the events of that type that pass all cuts, as well as the cross section uncertainty on that process.

Without a near detector, the errors from cross sections, for the case that there are no ν_μ oscillations, are 16%, which is equivalent to the statistical error for that case. For the case of mixing at the level indicated in the table, the statistical error on the probability would be 8%, while the errors from cross section uncertainties alone would be 31%.

In the case where there is a near detector that is identical to the far detector, one can try to cancel out these uncertainties. Consider first the prediction of the background events. The events in an identical near detector that pass the same analysis cuts as those made at the far detector can be described as

$$N_{near} = \Sigma_{i=e,\mu}\phi_i\sigma_i\epsilon_i M_{near} \quad (8)$$

And then one can use the simulation to predict the number of backgrounds at the far detector by the following equation:

$$B_{far} = N_{near}\frac{M_{far}}{M_{near}}R \quad (9)$$

where,

$$R = \frac{\Sigma_{i=e,\mu}\phi_{i,far}\sigma_i\epsilon_i}{\Sigma_{i=e,\mu}\phi_{i,near}\sigma_i\epsilon_i} \quad (10)$$

For different near detector off axis angles, there are different fractions of background events that pass all cuts, but at no value of the angle is the mix of backgrounds the same as that in the far detector. Figure 26 shows the fractional change in the variable R defined above due to the cross section errors listed in table 3. This translates directly into an uncertainty on the far detector background prediction due to current cross section uncertainties.

Note that for low off axis angles the systematic error due to the ν_μ charged current uncertainties is minimum, yet the error due to the neutral current and electron neutrinos is maximum there. Figure 27 shows the above errors added in quadrature, as a function of near detector off axis angle. Note that at best the cross section uncertainties can be reduced from 16% with no near detector to about 10% with an identical near detector, but given that this is only one of several systematic errors in the NOνA experiment, it is an unacceptably large fraction of the total error. The MINERνA experiment can significantly reduce the errors due to the charged current processes, because although it is on the NuMI axis where the neutrino flux is different from the off-axis fluxes, for the charged current processes the final state energy is close to the neutrino energy, and the flux prediction from the hadron production combined with NuMI horn B-field measurements means that charged current cross section channels will be measurable at the 5% level overall. So with the presence of MINERνA the error due to cross section uncertainties on the background at the far detector can be reduced from 10% to better than 5%. Furthermore, by measurements of charged current coherent pion production on axis one can infer the neutral current coherent pion process off axis using theoretical models constrained by the charged current process.

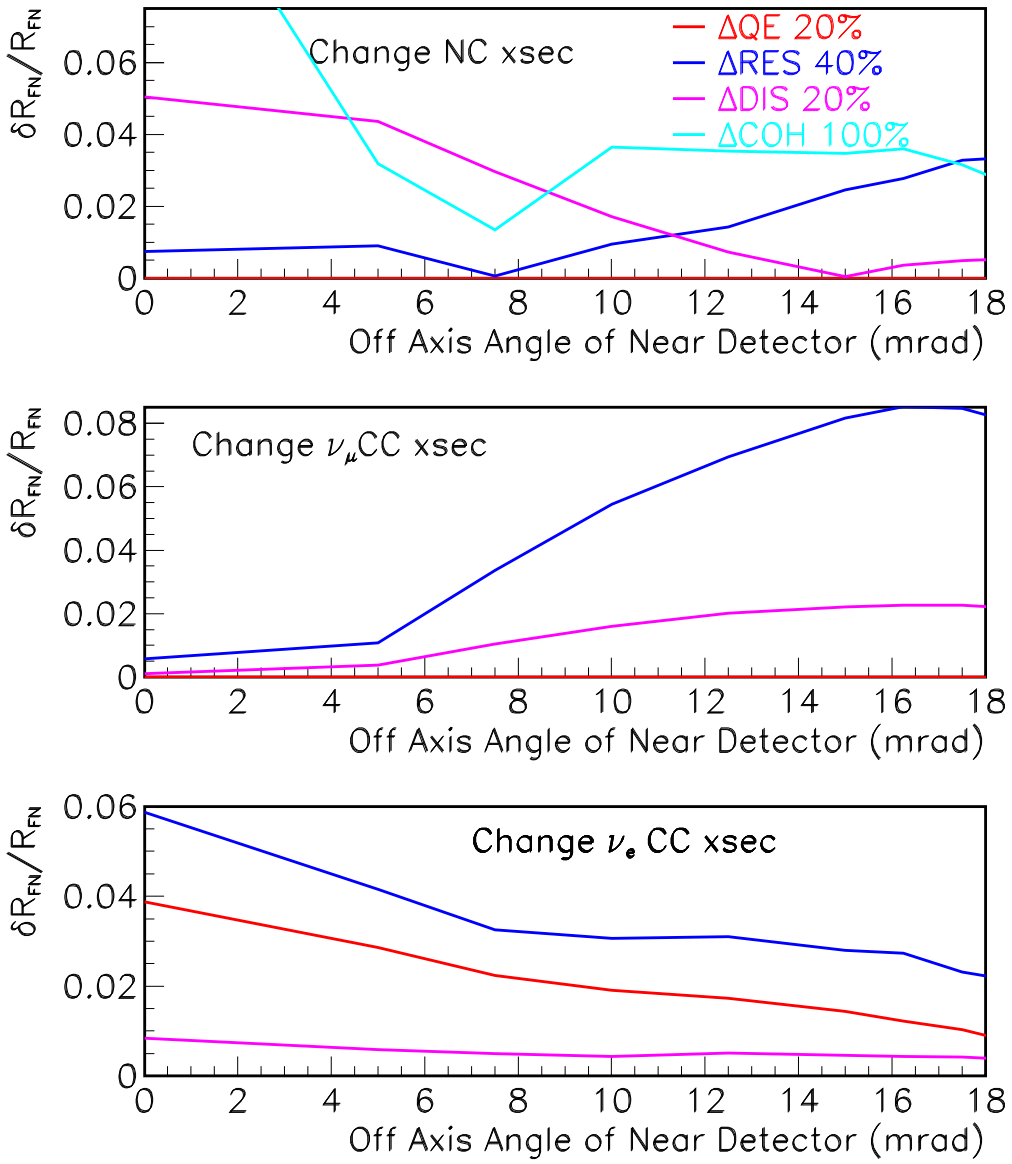

Figure 26: The fractional change in the far detector background prediction coming from an identical near detector, as a function of near detector off axis angle, for a far detector located 12km off the NuMI axis and 820km from Fermilab. The top plot shows the fractional change when the neutral current cross sections are varied by their uncertainties, the middle plot shows the fractional change when the ν_μ charged current cross sections are varied by their uncertainties, and the bottom plot shows the fractional change when the ν_e charged current cross sections are varied by their uncertainties.

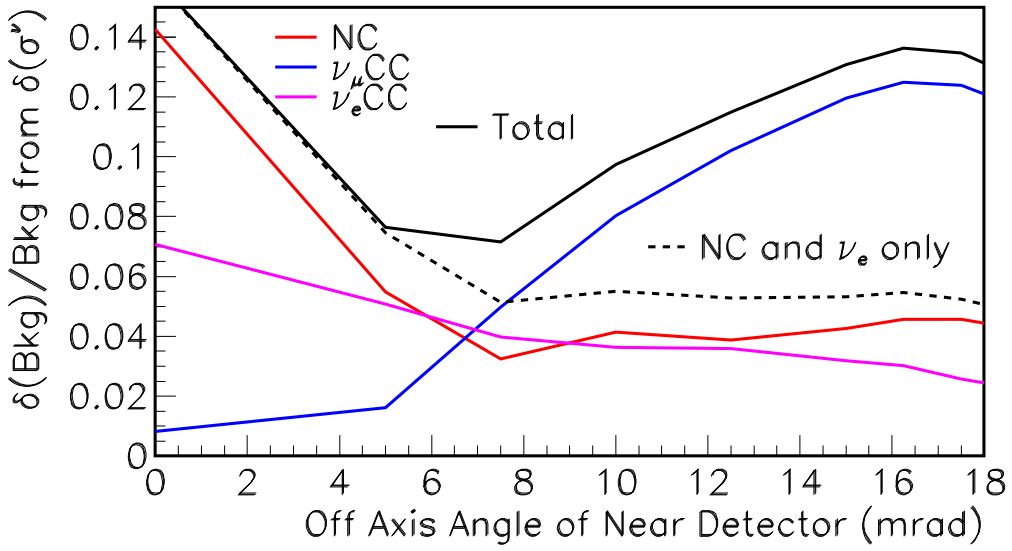

Figure 27: The fractional error in the background prediction at the far detector from uncertainties in each process (Quasi-elastic, resonance, deep inelastic scattering, and neutral current coherent π^0 production), added in quadrature for each source (NC, $\nu_\mu CC$, beam ν_e), plotted as a function of near detector off axis angle.

For the case where the number of signal events is well above the number of background events, the challenge to keep the uncertainties due to cross section errors low is even harder, since in that case the composition of events near to far is even more different than it is in the case of no signal events. Furthermore, because the total number of events is higher, the improved statistical precision will required an even more precise far detector prediction.

As a final note, it should be pointed out that the only cross section errors considered here are uncertainties in the overall levels of each of the processes. There is an additional uncertainty in the energy dependence of these processes, which will again contribute uncertainties in the far detector predictions because of the differing spectra.

6.3 Summary

This section has quantified how MINERνA's cross section measurements will have important consequences on both the current and future generations of neutrino experiments with the NUMI beamline. These improvements to MINOS and NOνA measurements are important regardless of the ultimate value of Δm^2 that MINOS measures, and regardless of the size of the $\nu_\mu \rightarrow \nu_e$ oscillation probability that NOνA ultimately measures.

References

[1] D. Drakoulakos *et al.* [the MINERνA collaboration], "Proposal to Perform a High-Statistics Neutrino Scattering Experiment Using a Fine-grained Detector in the NuMI Beam". `http://www.pas.rochester.edu/minerva/`.

[2] T. Kitagaki *et al.*, Phys. Rev. D26 (1983) 436.

[3] N.J. Baker *et al.*, Phys. Rev. D23 (1981) 2499.

[4] K.L. Miller *et al.*, Phys. Rev. D26 (1982) 537.

[5] D. Ashery et al., Phys. Rev. C **23**, 2173 (1993).

[6] for a review of pion absorption results see C.H.Q. Ingram, Nucl. Phys. **A684**, 122c (2001).

[7] M.K. Jones et al., Phys. Rev. C **48**, 2800 (1993).

[8] K. Garrow et al., Phys. Rev. C **66**, 044613 (2002).

[9] D. Rein and L. M. Sehgal, Nucl. Phys. **B223**, 29 (1983).

[10] E. A. Paschos and A. V. Kartavtsev, (2003), [arXiv:hep-ph/0309148].

[11] R. Merenyi *et al.*, Phys. Rev. D **45**, 743 (1992).